REPORT ARC-R-153

ROTARY, DEPLOYABLE SPACE SOLAR POWER SUPPLY

ASTRO
RESEARCH
CORPORATION
SANTA BARBARA, CALIFORNIA

Copy 23 of 50

Series 1

REPORT ARC-R-153

ROTARY, DEPLOYABLE SPACE SOLAR POWER SUPPLY

Submitted under Contract NASw-652

22 July 1964

Prepared by:

H. Schuerch

W. Robbins

ASTRO RESEARCH CORPORATION

P.O. Box 4128 • Santa Barbara, California

Telephone: 963-3423

CONTENTS

ILLUSTRATIONS

ABSTRACT

A generic review of space operations points towards the desirability of large-sized, lightweight surfaces, capable of deployment and precise contour control and orientation in the space environment.

Fresnel reflectors deployed by spin alone and maintained by spin in a precisely flat, circular disk which can provide high geometrical accuracy are investigated. Since no stiffness of the reflector is required or desired it can be made very thin and hence very light.

A passive heliotropic system, operating on solar radiation pressure, is proposed which is compatible with very lightweight, spin-stabilized construction.

The use of a deployable, solid-state-conventive-heat-transport device in the form of a rotating belt system is investigated. Preliminary experiments of heat transfer in vacuum are made.

Two sizes (15 KW and 150 KW) of rotary deployable space power supply are chosen to evaluate specific application of the above investigations. Modified Huettner turbines are proposed since they employ rotary boiler-condenser systems which, by centrifugal acceleration, eliminate many of the problems of heat transfer, vapor-liquid separation, and boiler feed normally encountered in space applications.

The proposed space power supplies are markedly superior to alternatives and it appears that a re-evaluation of the relative merits of the various approaches to space power generation would be in order.

1. INTRODUCTION

The concept of "deployable" structures may be applied, in principle, to the three basic forms of structural functions:

- Positioning of two or more locations relative to each other, such as implemented by beams, struts, trusses, etc.
- Enclosure of volumes, such as implemented by pressure vessels, space capsules, balloons.
- Provision of a surface for interaction with environmental matter or energy such as implemented by aerodynamic drag and lifting devices, shielding from meteorites or corpuscular energy, and reflectors, collectors or radiators of electro-magnetic energy.

The latter category is a particularly attractive candidate for deployable structures concepts because in space applications the surface areas required are frequently very large and structural loads are small. Thus, extremely thin-walled constructions can and must be employed in order to keep weights and associated systems costs at a tolerable level.

A curious analogy may be noted between the structural design problems associated with aircraft surfaces and collectors of electro-magnetic energy:

- In both cases, the structural forces are generated by impinging environmental momentum. (The analogy is complete in the case

of free molecular flow and photon pressure);

- In both cases, the design has to provide a relatively accurate contour aerodynamic profiles and surface smoothness in one case, appropriate optical geometry and surface reflectivity in the other; and
- In both cases the design must provide means of dynamic stability and control-ability. This involves flight path control in the case of aircraft, orientation and "pointing accuracy" (for instance, towards the sun for solar energy collection) in the case of reflectors.

The order of importance of the three basic requirements may vary within wide limits for the two types of applications. For instance, the forces generated by photon pressure are very small (approximately 10^{-9} lb/in^2 for perpendicular reflecting surfaces at earth's distance from the sun). They will provide a membrane stress of only 0.25 psi in a 1000 ft. focal length parabolic reflector supported at the rim, assuming that the mirror is made from a metallic film just thick enough (1,000 Å) to provide essentially zero transmission of light. Contour and attitude control requirements for high performance mirrors are measured in terms of minutes of arc, whereas similar requirements for parachutes, aerodynamic decelerators, etc., may be several orders of magnitude more tolerant. Finally, in the case of radiators, contour requirements are only of minor importance, as long as the overall geometry is such that mutual irradiation of surfaces ("view factor") is kept low.

Regardless of the individual differences in magnitude, similarities

of design approach can be observed for both types of structures. Airframes range from the conventionally rigid through discontinuous mechanisms (hinged flaps, helicopter rotors, "variable geometry" wings) to truly packageable-deployable (parachutes, "Rogallo wings," autorotating fabric structures). Similarly, solar collectors range from rigid, conventional-optics designs through various types of hinged petals and folding leaves to inflated or otherwise-contour-stabilized thin-film structures.

A truly packageable-deployable surface will need some means of maintaining the contour accuracy required for proper operation in the deployed state.

The conventional method of achieving dimensional accuracy is to provide rigidity in the structural material. This conflicts with the basic requirements for low weight and flexibility for packaging. The alternate means, compatible with flexible construction is to employ a controlled interaction of the structure with a force field, which is supplied either by the vehicle or by the environment. An almost perfect, everyday example of this is a soap bubble. Its dimensional accuracy is provided by interaction of a completely non-rigid "structural material" (liquid) with a force field (surface tension and internal pressure), forming a very nearly perfectly spherical, thin-walled shell.

In a search for suitable force fields for contour control of space solar concentrator reflectors, those generated by rotation of the vehicle (with respect to the distant fixed stars) are particularly attractive. Centrifugal

forces are achieved and maintained simply by maintaining rotational motion of the vehicle.

Rotation of the vehicle will, however, have effects upon the other components of a space solar power plant. These are the orientation mechanisms required to point the collector axis towards the sun with sufficient accuracy, the thermodynamic power generator which converts the collected and concentrated solar energy into useful mechanical power, and the radiator which rejects the waste energy of the thermodynamic cycle back to the space environment.

It is necessary, therefore, to examine the systems implications of rotary deployment and contour stabilization for solar collectors. Such an examination shows, that these other systems components can be designed to benefit from the presence of rotational motion. Thus, an overall concept can be evolved which employs to advantage the inertial rotation of the vehicle.

The result of this study is a unique system built around the concept of employing centrifugal and precessional forces inherent in rotary motion.

II. GENERAL DESCRIPTION OF SYSTEM

Two sizes of solar space power supplied have been selected arbitrarily for detailed studies. One is designed for 15 KW, the other for 150 KW electrical output. Figures 1 through 4 show the configurations for the two selected sizes in folded and deployed condition. Figures 5 and 6 show some of the details of the 150 KW-system. The basic components of the system are.

- the deployable solar concentrator and reflection system,
- the rotary mercury steam engine (Huettner turbine),
- the electrical power generator (alternator) and its associated radiation cooler,
- the heat rejector, built as a rigid, elongated conical radiator for the 15 KW size, augmented by a deployable solid state convective heat transport device in the form of a running belt system for the 150 KW size, and
- the passive, heliotropic orientation system in the form of the peripheral torquing and modulating vanes located at the reflector rims.

A summary of sizes, weights and operational parameters for the two selected sizes is given in Table I.

The features of the various subsystems are described in the subsequent sections.

Table 1. Solar Power Supplies - Summary of Design Data

(1) OUTPUT (KW)		
Electrical	15	150
Turbine Shaft Output	17.7	170
(2) DIMENSIONS (ft)		
Diameter — deployed	50	190
— folded	8.3	11
Length — deployed	28	52
— folded	28	26
(3) ROTATIONAL SPEED (rpm)		
Mirror	-6	-12
Boiler	+317	+210
Turbine	-23,700	-11,790
Belt	--	+24
(4) SOLAR COLLECTOR DATA		
Primary Mirror Area, ft^2	1500	17,158
Concentration Ratio (Theoretical)	100	120
Concentrator Efficiency	0.8	0.66
Absorber Efficiency (Utilization Ratio)	0.66	0.70
(5) MERCURY CYCLE DATA		
Boiler	1097°F	300 psia
Turbine Inlet	1150°F	115 psia
Condenser	620°F	8 psia
Efficiency ($\eta_{Rankine} \times \eta_{Turbine}$)	17.3%	
(6) WEIGHTS (lb)		
Mirrors and Drive System	65	558
Boiler	18	87
Condenser	94	326
Belt System	--	264
Working Fluid	12	68
Turbine and Alternator	30	150
Housing, Ducts, etc. (Including Alternator Cooler)	26	135
Total Weight	245	1,588
(7) POWER/WEIGHT RATIO (KW/lb)	0.061	0.094
Specific Weight (lb/KW)	16.4	10.6

III. CENTRIFUGALLY DEPLOYED FRESNEL REFLECTOR

A. STATE OF ART OF SOLAR CONCENTRATORS FOR SPACE APPLICATIONS

A review of the recent literature concerning solar concentrators for space applications (see References 1 through 6) shows that a wide variety of approaches to the problem have been implemented or proposed. The reflecting surfaces employed have been parabolic, spherical, cylindrical, conical, Fresnel type, and various combinations and modifications of these. The desired geometrical shapes have been obtained by the use of rigid structures (either one-piece or foldable), petals, umbrella structures, inflatable structures permanently pressurized, and inflatable structures whose long-term shape is maintained by rigidizing with foam plastic.

In general, the rigid structures are capable of concentration ratios of a few thousand while the others are capable of concentration ratios of a few hundred. The weights per projected area of collecting surface lie in the region of a few tenths of a pound per square foot to a few pounds per square foot except for inflatable structures which might have a weight as low as 0.03 pounds per square foot. However, inflatable structures are vulnerable to leakage because of puncture by meteoroids and are, therefore, not applicable to long-term applications in space.

None of the systems generally proposed is well suited to the large-

sized power supplies considered in this study. The requirement here is for the collection of large amounts of power with a low total weight by a structure that can be folded into a small volume. Only moderate concentration ratios are necessary because of the relatively low boiler temperatures utilized.

B. SPINNING FRESNEL CONCENTRATORS

The proposed advanced thermodynamic space solar power supply systems employ a very thin Fresnel reflector modified so as to bring sunlight to focus in the toroidal boiler space of the Huettner turbine. This is accomplished by supporting a thin Fresnel surface with very narrow grooves upon a spinning isotensoid filamentary disk.

The "Fresnel Mirror" is an adaptation of the well-known Fresnel lens (References 1 and 4). The reflector proposed here consists of a thin film of plastic material provided with circular grooves of sawtooth section, in appearance very much like a phonograph record, and aluminized to provide optical reflectivity. (See Figures 7 and 13.)

Previous work (Reference 7) has shown that a spinning isotensoid disk formed by a network of flexible filaments constitutes an optimum design of minimum weight for a given covered surface area and peripheral speed, and that the deformation from centrifugal forces is isotropic because of the uniform biaxial strain corresponding to the uniform stress in all fibers. Such a construction allows a very flexible reflector which can be packaged into a small volume. It can be deployed by spin alone and maintained by spin in a precisely flat circular disk which can provide almost any desired degree of

geometrical accuracy. Since no stiffness of the sheet is required to obtain the desired shape, it can be made very thin and hence very light. It is essentially invulnerable to micrometeoroids since a puncture of the mirror film will affect a negligibly small area and an improbable direct impact upon a structural filament will alter the geometry of only a very small fraction of the total reflector.

In practice, the Fresnel mirror might consist of a sheet of "Mylar" or similar plastic film with an average thickness of 0.002 inch with grooves ranging from a width of 0.010 inch near the center to 0.002 at the edge. In order to increase resistance to the space environment, the film can be aluminized on both faces. For ease of fabrication, the reflector is divided into segments which are easily fabricated with a conventional press and embossing tool. The sections are fastened to an isotensoid disk of synthetic fiber. For disks spun with peripheral speeds of 1500 feet per second, the filamentary disk would weigh approximately the same as the film. For lower peripheral speeds, considerably less net weight can be used. A 2-mil aluminized "Mylar" sheet has a mass of 0.0125 lbm/ft^2. The total reflector weight will thus be in the general region of 0.015 to 0.025 lbm/ft^2.

C. GEOMETRICAL CONCENTRATION EFFICIENCY

Shown in Figure 7 is a schematic cross-section of a Fresnel reflector designed to focus solar radiation into the toroidal space occupied by the absorber boiler surface of the Huettner turbine. It can be seen that a certain portion of the mirror's projected area (projected onto a plane parallel to

the mirror) is ineffective because the back side of each sawtooth annular groove is shaped to prevent shading of absorber by the adjacent reflecting surface. From this figure, it can be seen that if the groove shown is of unit depth, then there is an effective annular area of $2\pi R/\tan\frac{\theta}{2}$ and a shaded annular area of $2\pi R \tan\theta$. The geometrical concentration efficiency, η_g , is then defined as the ratio of effective area to total area in the reflecting surface:

$$\eta_g = \frac{1}{\pi (R_2^2 - R_1^2)} \int_{R_1}^{R_2} 2\pi R \, \frac{\cot\frac{\theta}{2}}{\cot\frac{\theta}{2} + \tan\theta} \, dR \quad .$$

Manipulation yields

$$\eta_g = \frac{2}{(R_2^2 - R_1^2)} \int_{R_1}^{R_2} R\cos\theta \, dR = \frac{2}{R_2^2 - R_1^2} \int_{R_1}^{R_2} \frac{Rf \, dR}{[f^2 + (R - R_a)^2]^{1/2}}$$

which upon integration leads to

$$\eta_g = \frac{2f^2}{R_2^2 - R_1^2}\left\{\sqrt{\left(\frac{R_2 - R_a}{f}\right)^2 + 1} - \sqrt{\left(\frac{R_1 - R_a}{f}\right)^2 + 1} + \frac{R_a}{f} \ln \frac{\sqrt{\frac{R_2 - R_a}{f} + \left(\frac{R_2 - R_a}{f}\right)^2 + 1}}{\sqrt{\frac{R_1 - R_a}{f} + \left(\frac{R_1 - R_a}{f}\right)^2 + 1}}\right\}$$

The geometrical concentrating efficiency of a Fresnel reflector as a function of R_2/f for $R_1 = R_2/2$ and $R_a = 0$ and $0.1f$ is shown in Figure 8. It is seen, that for aperture ratios R_2/f greater than unity, the geometrical "Fresnel loss" becomes significant.

The reflector or mirror system for the 150-kilowatt power supply is shown as a schematic cross-section in Figure 9. The primary reflector is a Fresnel mirror extending from an inner radius of 36.6 feet to an outer radius

of 95 feet. The region between radii of 80 and 95 feet is divided into 180 radial strips which act both as part of the concentrator and as modulating vanes for the heliotropic orientation system which is discussed later. The secondary reflector extends from a radius of 18.5 feet to a radius of 43 feet, the entire surface being plain but with the region between 36.6 feet and 43 feet being divided into 180 strips to act both as a secondary reflector and as torquing vanes for the orientation system. Two small tertiary reflectors are mounted directly on the boiler and increase considerably the region in which the boiler can accept radiation from the secondary reflector.

For both reflectors, it is assumed that the reflecting film is "Mylar" of 0.002 inch average thickness and a density 1.2 gm/cm^3. Each reflector is supported on a filamentary isotensoid disk of one-half the mass of that of the film it supports and with a moment of inertia corresponding to a constant area density. The hubs are each assumed to have a radius of 6.5 feet and be of constant thickness.

As can be seen in Figure 9, various regions of the projected area of the concentrator are useful to different fractions in contributing to solar radiation received at the boiler. The total effective projected area is computed in Table II to be 17,158 ft. Values of the geometrical efficiency, η_g, resulting from Fresnel shading have been computed for the various sections by the relationship derived earlier and are also shown in Table II. The total of $A_p \eta_g$ shown in the table is the area which multiplied by the sun's irradiance (solar constant) would give the energy arriving at the boiler, if the reflectivity of all reflector surfaces were unity.

Table II. Effective Concentrator Area of 150-KW System

Inner Radius (ft)	Outer Radius (ft)	Fraction of Area Effective in Concentration	Effective Projected Area A_p (ft^2)	η_g	$A_p \eta_g$ (ft^2)
36.6	43	0.50	801	0.92	737
43	80	1.00	14,300	0.84	12,020
80	95	0.25	2,057	0.73	1,502
			Total 17,158		Total 14,259

As shown elsewhere, the net power, P_b, into the boiler is then

$$P_b = H (A_p \eta_g) r_m^2 a_b \eta_a = H A_p \eta_c \eta_a$$

where H = solar irradiance (solar constant) = 0.129 kw/ft^2

A_p = effective projected area concentrator

η_g = geometrical concentration efficiency

r_m = reflectivity of mirror surfaces = 0.95

a_b = absorbtivity of boiler = 0.88

η_a = utilization factor (accounting for re-radiation) = 0.70 .

The overall concentration efficiency is 0.66 and the net power delivered to the boiler is 1020 kilowatts.

D. ANALYTICAL DESIGN FOR NET-SUPPORTED REFLECTOR

The analytical design for a constant-stress spinning net presented in Reference 7 assumes that the mass loading of the filament is uniform. In the case of the net-supported reflecting film, an additional term needs to be

considered to account for the mass associated with the film itself. Figure 10 shows an element of the net with its applied forces.

Introducing the condition that the filament force, T , remain constant throughout ($dT/d\ell = 0$) yields a relationship defining the net geometry as follows:

$$\frac{\rho}{r_o} = \frac{\sin\beta}{\Omega R\,(1 + \mu R \cos\beta)}$$

where β = angle between fiber and radial

ρ = radius of curvature of filament

r_o = peripheral radius of disk

m' = mass/unit length of fiber

M' = mass/unit area of film

ω = rotational speed

T = fiber tension

n = number of fibers in each system

and where these terms are collected into the non-dimensional groups:

$$R = r/r_o$$

$$\Omega = m'\,\omega^2\,r_o^2/T$$

$$\mu = M'\,\pi\,r_o/2\,m'\,n \quad .$$

This expression can be integrated to eliminate ρ , yielding a differential equation for β :

$$\frac{d\beta}{dR} = \frac{1}{\cos\beta}\left[\frac{\Omega R\,(1 + \mu R\cos\beta)}{\sin\beta} - \frac{\sin\beta}{R}\right] .$$

Solutions to these equations can be obtained either by graphical or digital methods. Figure 11 shows a polar plot of the net geometry for the case $\mu = 1$, $\Omega = 1.5$. Two types of solutions are observed, differing in character according to the specific values of μ and Ω used, as shown in Figure 12. The first type is "cusped," i. e. the filament path terminates in a radial direction at a radial distance $R > 0$. The second type is "looped," i e. the filament path is continuous, looping around the axis to a minimum radius. The case of transition between the two solutions allows a net with zero hub radius, since the filaments all intersect the axis.

A discussion of the significance of the tip speed parameter Ω is in order. The peripheral speed ωr_o of the structure is limited by the specific strength $T/m'g$ of the filament, thus:

$$\omega r_o = \sqrt{g \Omega \left(\frac{T}{m'g}\right)} \quad .$$

For the case $\Omega = 1$, the net degenerates into a circular hoop. For Ω-values higher than unity, the peripheral speed can be increased over that possible for a single hoop by the factor $\Omega^{1/2}$. Figure 12 indicates that for μ-values of the order of unity (net weight approximately equal to film weight), and for small hub radii, Ω-values of the order of 1.4 can be achieved. For a high tenacity polyester fiber ("Dacron"), specific strength values of 2×10^5 ft. are available. Using a safety factor of 16 (corresponding to an elastic strain of approximately .5%) the peripheral disk velocity becomes

$$\omega r_c = \left[g \Omega \frac{\text{specific strength}}{\text{safety factor}} \right]^{1/2} \approx 750 \text{ ft/sec} \quad .$$

Lower strain values can be obtained by either smaller peripheral velocities

or by the use of a higher-modulus fiber such as metal or glass. Conversely, lower peripheral velocities can be used by employing a higher μ-value, i. e. a lower weight net for support of the reflecting film.

The characteristic strain in the spinning disk causes the supported film to be subject to uniform bi-directional (i. e. isotropic) tension. Thus, the condition of stress and strain in this device is analogous to that found in an inflated spherical membrane or "soap bubble." Previous experiments with aluminum-plastic composite films (Reference 8) indicate that biaxial strains of the order of .05% are required to eliminate residual wrinkles stemming from the packaging operations. Control of the peripheral speed can be employed to achieve complete stretching and, therefore, accurate geometrical control of the reflecting disk surfaces. In the case where the reflecting surface is provided with a Fresnel pattern, the pattern geometry can be adjusted to account for the membrane stretching associated with spin.

E EXPERIMENTS

A number of preliminary experiments have been conducted relating to fabrication technique, optical characteristics and folding-deployment mechanics of net supported mirror surfaces. Plastic films made from PVA solution were sprayed upon prepared surfaces of glass and of a brass block with machined Fresnel-groove patterns. A filamentary net made from 8-lb. test heat-stretched Type 52 Dacron was placed over the original film and a second layer of solution applied. This causes the net to be firmly embedded in the resulting film of 1 to 2 mil total thickness.

After hardening of the film the assembly is peeled off and vacuum plated with aluminum to a coating thickness of approximately 1000 Å on both sides. The grooved sample was designed with uniform groove angles of $22\text{-}1/2^{\circ}$, causing normal incident light to be concentrated into an axial pencil. Figure 13 shows this mirror with a white screen placed into an axial plane, visualizing the geometry of the concentrated, light rays.

Several other disks of various dimensions were made. An annular mirror, such as proposed for the 150 KW system, is shown expanded in Figure 14 and folded in Figure 15. Two methods of folding the mirror are shown in Figures 16 and 17. In either case, the absence of the reflecting surface near the hub materially eases folding.

IV. HELIOTROPIC ORIENTATION SYSTEM

A. GENERAL DISCUSSION

The successful operation of a space solar power supply of the type under consideration requires that a space vehicle, probably a satellite of the earth, be maintained with a particular axis pointed toward the sun with reasonable accuracy and for a period of time which could span several years.

The problem of orienting a space vehicle with one axis always toward the sun appears simple at first glance since the forces encountered are very low by most standards. However, especially in the vicinity of the earth, there are a considerable number of influences that could alter the attitude of the vehicle when they are allowed to act for a period of hours or days.

Almost every influence which might act adversely in affecting a space vehicle's orientation might also, if appropriately controlled, be used to control attitude. Some of these influences are the ejection of mass, aerodynamic forces, solar radiation pressure, solar wind, the earth's gravitational field, the earth's magnetic field, angular acceleration of flywheels, and the precession of gyroscopes. Because of the requirement for simplicity and reliability, influences for attitude control which are not applicable to passive systems have been rejected as impractical, this leaving only radiation

pressure and solar wind as suitable candidates. Since pressure from solar wind is considerably lower than that from radiation, it is not considered separately. Aerodynamic forces and the earth's gravitational and magnetic fields are considered as potential sources of disturbing influence.

One important factor to be considered for the space solar power supply is that various portions of the system will be spinning at relatively high angular velocities in order to cause flexible structures to be accurately deployed, and to pump working fluid for the thermodynamic cycle. Since the solar concentrator will have a considerable surface area and have a large polar moment of inertia (about its axis of symmetry), the possibility exists that the system can have a very large angular momentum about its polar axis. If the power supply is to be an earth's satellite, its angular momentum must be completely reversed (rotated through 180°) every six months. Even though the precession rate required is quite small (1.99×10^{-7} rad/sec), the required torques can turn out to be surprisingly large.

B. AERODYNAMIC FORCES

If the space solar power supply is an earth's satellite, aerodynamic moments may be of considerable significance for orbits where aerodynamic drag limits orbit lifetime to a few years (or even tens of years). Such moments will not be in the correct direction to cause heliotropic behavior but will rather lie normal to both the satellite axis of symmetry and the orbit path. However, aerodynamic moments will adversely affect whatever attitude control system is used.

To evaluate the aerodynamic moment on the space solar power supply, consider the simplified configuration shown in Figure 18, where a circular disk is connected to a point mass (equivalent to the total mass at the center of gravity). In the highly rarefied atmosphere in the region of interest the Knudsen number will be much less than unity. It is assumed that the gas molecules stick to the surface and subsequently leave diffusely at a relatively low speed. The ratio of vehicle speed to average molecular speed is assumed to be very large. Under these conditions the lift is zero, and the drag is given by

$$D = \rho v^2 A \cos\theta = D_o \cos\theta$$

and there is a restoring torque on the system of

$$T = D\ell \sin\theta = D_o \ell \sin\theta \cos\theta \quad .$$

The drag on an earth's satellite in circular orbit at an altitude of 350 miles is taken from Reference 9 to be 3×10^{-8} lb/ft^2.

Let $\ell = 10$ meters

$A = 1386$ m^2

Then

$$D_o = 2.0 \times 10^{-4} \text{ kg} = 19.6 \times 10^{-4} \text{ Newton}$$

and

$$T_{max} = 9.8 \times 10^{-3} \text{ Newton} \cdot \text{meter} \quad .$$

If, during a time, the attitude control system does not function, such as when the satellite is in the shade of the earth, this torque could disturb the satellites attitude. As an example, assume that the maximum torque above acts upon a satellite with zero spin momentum and a pitch moment of

inertia of 75×10^3 kg · m^2 for a period of 45 minutes.

Then

$$\ddot{\theta} = \frac{T}{I} = 0.131 \times 10^{-6} \text{ rad/sec}^2$$

and after 45 minutes

$$\dot{\theta} = 0.353 \times 10^{-3} \text{ rad/sec}$$

$$\theta = 0.477 \text{ rad} .$$

This is an intolerably large angular error. Even though the conditions chosen are rather extreme, the problem will be quite serious for satellites in low orbit (below 500 miles) which have low angular momentum unless the system is specifically designed to minimize the effect by placing the center of gravity at the center of aerodynamic pressure.

C. EARTH'S GRAVITATIONAL FIELD

Because of the gradient of the gravitational field experienced by an earth's satellite there is a torque about the three principal axis which depends upon the moments of inertia about these axes and upon the orientation with respect to the earth. If, however, these three moments of inertia are all equal the torques all become zero.

Since it is desired that the space solar power supply be heliotropic rather than geotropic, torques resulting from the earth's gravitational field offer no promise of being adaptable for the present purpose. However, such torques can be undesirable disturbances which must be met by the orientation system.

An earth's satellite in a circular orbit and with an axis of symmetry

(resulting in two equal moments of inertia about any two orthogonal axes normal to the axis of symmetry) is assumed to be oriented with its axis of symmetry (X-axis) normal to the orbit trajectory and at an angle above the horizontal.

Let $I_x > I_y$

$I_y = I_z$.

Then there is a torque from the gradient of the combined acceleration field (gravitational and centrifugal) in the direction of the orbit (y-direction) which is given by

$$T_y = 4\,\omega_o^2\,(I_x - I_z)\,\sin\theta_y\,\cos\theta_y$$

where $\omega_o = \sqrt{g_o\, r_o^2 / r^3}$ = angular frequency of the satellite in its orbit

r_o = earth's radius - 20, 850, 000 ft

g_o = gravity at earth's surface = 32.2 ft/sec^2

r = radius of circular orbit .

At an elevation of 500 miles

r = 23, 490, 000 ft

$\omega_o^2 = 1.086 \times 10^{-6}$

$\omega_o = 1.04 \times 10^{-3}$

τ_o = 6,040 sec = 100.7 min .

At this elevation a maximum torque about the y-axis occurs when $\theta_y = \frac{\pi}{4}$ and is

$$T_{y_{max}} = 2\,\omega_o^2\,(I_x - I_z) \quad .$$

Letting $I_x = 75,000$ kg · m^2

$I_z = 50,000$ kg · m^2

results in

$$T_{y_{max}} = 0.054 \times 10^{-3} \text{ Newton} \cdot \text{meter} .$$

As shown later, this torque is considerably more than that obtained from the system for orientation by solar radiation pressure. However, this is the peak value of a torque which varies cyclicly as the satellite orbits the earth and which will cause no net change in angular momentum of the satellite. Further, the torque varies as $1/r^3$ from the center of the earth, its value becoming quite small at a distance of a few tens of thousands of miles from the surface of the earth.

D. EARTH'S MAGNETIC FIELD

The rotation of a conducting surface in a magnetic field will, in general, cause currents to be induced in the conductor and the interaction of these currents with the magnetic field will cause torques on the conducting surface.

For an earth satellite in a circular orbit of about 500-mile altitude, the earth's magnetic field has a peak value of about 0.3 gauss. Depending upon the momentary angle between the orbit plane and the earth's magnetic axis, the vector field in the vicinity of the satellite will remain nearly constant, rotate twice per orbit period, or exhibit some intermediate behavior.

The major effect of the earth's magnetic field upon the space solar power supply will be one of spin damping, or torquing about the spin axis. According to Smythe (Reference 10) the retarding torque T per unit of length

of a thin circular cylinder of area resistivity $2\pi R$ and radius a, spinning on its axis with an angular velocity ω in a uniform magnetic field, B, normal to its axis is

$$\frac{T}{\ell} = \frac{1}{2} \frac{\omega a^3 R B^2}{(R^2 + \omega^2 a^2)} .$$

In order to evaluate what torque might exist on the condenser of a solar power supply, consider it to be a stainless steel cylinder with a diameter of two meters and a wall thickness of 0.015 cm. The electrical resistivity of the stainless steel is taken to be 50×10^{-6} ohm-cm. Assume that the magnetic field is always oriented normal to the satellite spin axis (giving the largest possible torque).

Summarizing:

ρ = resistivity = 50×10^{-6} ohm-cm

t = thickness = 0.015 cm

a = radius = 1.0 meter

B = 0.3 gauss

ω = 15.7 rad/sec .

By definition $2\pi R = \rho/t$

and $R = 5.3 \times 10^{-4}$ ohm .

Rewriting the equation for torque per unit of length gives

$$\frac{T}{\ell} = \frac{\omega a^3 B^2}{R\left(1 + \frac{\omega^2 a^2}{R^2}\right)} .$$

When $\omega^2 a^2 / R^2$ is evaluated in electromagnetic units, it is much less than unity and

$$\frac{T}{\ell} = 1330 \frac{\text{gauss}^2\ \text{m}^3}{\text{ohm} \cdot \text{sec}} = 13.3 \times 10^{-6} \text{ Newton} .$$

In the period of a year ($\Delta t = 31.5 \times 10^6$ sec)

$$\frac{\Delta h}{\ell} = \frac{f\,\Delta t}{\ell} = 418 \frac{m\ kg}{sec}$$

and if ℓ is several meters, Δh may be a significant portion of the angular momentum that can be satisfactorily precessed by solar radiation pressure.

For a situation with zero spin momentum, the primary reflector might be torqued to significant degree normal to the axis of symmetry if it were a single conductor. However, its division into insulated units allows the total torque from the earth's magnetic field to be reduced to $\frac{1}{n^2}$ of its undivided value, where n is the number of divided units. Hence, this torque can be made as small as desired.

E. SOLAR RADIATION

Radiant energy carries with it a momentum equal to the energy divided by the speed of light

$$F\,\Delta t = U \cdot \frac{1}{c} .$$

If this energy is absorbed by a surface normal to the radiant flux, there is a corresponding pressure

$$p_s = \frac{F}{A} = \frac{1}{A}\frac{dU}{dt}\frac{1}{c} = \frac{P}{A}\frac{1}{c} = \frac{H}{c}$$

where F = force

Δt = time interval

U = energy

c = speed of light

A = area illuminated

P = power

H = irradiance, or "solar constant"

$p_s = 4.5 \times 10^{-5}$ dyne/cm^2 = 4.5×10^{-6} Newton/m^2 .

If the energy is reflected, there is an additional pressure corresponding to the reflected energy.

If a space vehicle is designed so that the solar pressure produces a torque in a direction opposite to the rotation which causes the torque, a vehicle with zero spin angular momentum will execute an undamped plane oscillation about the desired orientation. If some means for damping the oscillations is provided (such as a viscously mounted flywheel), the system will point toward the sun at all times if other disturbances are absent.

If the system has considerable spin angular momentum the above torque will cause the spin axis to precess about the direction to the sun, the spin axis describing a cone. In order to cause such a system to rotate so that its axis points at the sun, the applied torque should be normal to both the angular momentum and the desired rotation.

As an example of the torque from radiation pressure on a space vehicle with no spin momentum, consider the simplified situation shown in Figure 19 where a circular disk is connected to a point mass.

If all the solar energy impinging upon the disk is either absorbed at the disk or reflected and subsequently absorbed elsewhere in the system (none is reflected back into space), then the force on the system is the same as if all the energy had been absorbed at the disk.

Therefore $$F_s = p_s A \cos\theta$$

$$T = \ell A p_s \sin\theta \cos\theta$$

and for small θ

$$\frac{\partial T}{\partial \theta} = \ell A p_s = 6.23 \frac{\text{Newton} \cdot \text{meter}}{\text{radian}} .$$

The period of free oscillation about the direction to the sun is

$$\tau = \frac{2\pi}{\omega} = 2\pi \left[\frac{I}{\frac{\partial T}{\partial \theta}} \right]^{1/2} = 6.9 \times 10^3 \text{ sec} = 1.92 \text{ hours}$$

The torque from radiation pressure is thus quite substantial and could, if damping were provided, suffice for stabilizing the system in regions away from the earth where aerodynamic force, gravitational effects, and magnetic effects are small, and where the system will not be shaded from the sun part of the time.

Louis Ule (Reference 11) has presented a method for orienting spinning satellites by radiation pressure. According to Ule, the torque obtained from an annular array of mirrors as shown in Figure 20 with the angular separation of the bases equal to the angle subtended by the bases themselves is

$$T_s = \frac{4}{3} p_s (R_o^3 - R_i^3) \sin 2\theta$$

where p_s = solar radiation pressure for absorbing surface

θ = angle between spin axis and line to sun

R_o = outer radius of array

R_i = inner radius of array .

In general, if the axial mirrors extend on either side of the base

for a distance k times the arc of the base at that radius (instead of the factor 2.0 which Ule used), then

$$T_s = \frac{k\pi}{6} p_s (R_o^3 - R_i^3) \sin 2\theta \quad \text{for} \quad \tan\theta < \frac{1}{2} \quad .$$

In order to determine what torque would be available if Ule's system were applied to a space solar power supply, let

$$R_i = 21 \text{ meters}$$

$$R_o = 22 \text{ meters}$$

$$\theta = 0.02 \text{ radians} = 1^\circ \qquad \text{(an assumed allowable tracking error)}$$

which, upon substitution gives

$$T_s = 2.58 \times 10^{-4} \text{ Newton} \cdot \text{meter} \quad .$$

The torque is quite low but could be increased by increasing k , thus decreasing the θ at which maximum torque occurs but increasing the torque for a given small θ . A factor-of-ten increase would be possible if $\theta_m \simeq 2^\circ$ (twice the allowable tracking error). However, the system with large values of k requires that large mirror areas be maintained parallel to the axis of symmetry and it could not be designed as a lightweight structure.

However, a system is proposed below which has a similar torquing behavior but which requires much less total mirror surface and can be designed as a lightweight, flexible, spin-stabilized structure.

F. A PROPOSED METHOD FOR HELIOTROPIC ORIENTATION BY RADIATION PRESSURE

Consider a spinning heliotropic satellite with two sets of vanes as

shown in Figure 21, the second set being displaced from the first by one-half of a vane width. In order to facilitate discussion and preliminary analysis, it will be assumed that sunlight is columnated. Half the solar radiation passes through the first set of vanes but causes no torque on this set. As long as the axis of symmetry of the system is pointed toward the sun, one-half of the radiation which passes through the first set of vanes will strike the second set as is shown in Figure 22. However, if the spin axis is deviated from the direction to the sun, the second set of vanes will be illuminated over varying amounts of their surface as can be seen in Figure 23.

The front and rear sets of vanes will be called modulator and torqueing vanes, respectively.

If the system is observed along the axis about which it has been rotated to deviate its axis of symmetry from the sun, the vanes at this point are illuminated as shown in Figure 24. In this figure

w = width of vanes and space between vanes at the radius R

ℓ = distance between two sets of vanes

θ = angle between axis of symmetry and direction to sun .

Within an increment of radius ΔR the axial component of force from radiation pressure on a black vane in the position shown in Figure 24 is

$$f_{a_1} = p_s \left(\frac{w}{2} + \ell \tan\theta\right) \cos^2\theta \, \Delta R \quad \text{for} \quad \tan\theta < \frac{w}{2\ell}$$

and at the opposite side of the disk the axial force on a vane is

$$f_{a_2} = p_s \left(\frac{w}{2} - \ell \tan\theta\right) \cos^2\theta \, \Delta R \quad \text{for} \quad \tan\theta < \frac{w}{2\ell} \quad .$$

Let there be N vanes ($\frac{N}{2}$ vane pairs) . The entire annular ring between two radii is covered by spaced vane pairs between $\theta = -\frac{\pi}{2}$ and $\theta = \frac{\pi}{2}$. The torque on the pair of vanes on the axis of θ rotation is

$$T_1 = (f_{a_1} - f_{a_2}) R = p_s \cdot 2\ell \sin\theta \cos\theta \cdot R \, \Delta R$$

and the component of torque in this same direction that is contributed from a vane pair at the angle ϕ is $T_1 \cos^2\phi$,

where ϕ = angle measured about axis of symmetry from position of torquing vane with maximum illumination .

Then from R_i to R_o and $\phi = -\frac{\pi}{2}$ to $\phi = +\frac{\pi}{2}$

$$T = p_s \cdot 2\ell \sin\theta \cos\theta \int_{R_i}^{R_o} R dR \cdot \frac{N}{2\pi} \int_{-\frac{\pi}{2}}^{\frac{\pi}{2}} \cos^2\phi d\phi \quad \text{for} \quad \tan\theta < \frac{w_{min}}{2\ell}$$

$$T = p_s \cdot \frac{N\ell}{4} (R_o^2 - R_i^2) \sin\theta \cos\theta \quad \text{for} \quad \theta < \frac{\pi R_i}{2N\ell} .$$

If N is large (θ_{max} small) , then

$$\sin\theta \cos\theta \simeq \tan\theta$$

and

$$T_{max} = p_s \frac{\pi}{8} R_i (R_o^2 - R_i^2) .$$

Further, if $R_o \simeq R_i$

$$T_{max} \simeq p_s \cdot \frac{\pi}{4} R^2 \Delta R .$$

If the torquing vanes are made specularly reflecting instead of black and are canted slightly so that the reflected radiation misses the modulator blades, the precessing torque will be approximately doubled.

In order to evaluate what effect system size would have upon the operation of the proposed heliotropic orientation system, the following assumptions concerning scaling will be made:

a) The various reflector systems, including the vanes of the heliotropic system are geometrically similar, as far as their gross surface characteristics are concerned.

b) The thickness of reflector film is constant and is not a function of system size. The mass per unit of area, ρ_A, is therefore fixed

c) The ratio of parasitic weight (reflecting surfaces) to weight of the filamentary isotensoid disks is the same for all systems.

d) The filaments are stressed to the same fixed design value in each case by having the same tip speed, v_t

e) The angular momentum of all other portions of the system are negligible compared with that of the reflector system.

Under the above assumptions mass of the system will be proportioned to the radius, r, squared and the moment of inertia will be

$$I = k_1 \frac{\pi}{2} \rho_A r^4$$

where k_1 depends upon the geometry and the ratio of parasitic weight to filament weight. Then the angular momentum, h, is

$$h = I\omega = I \frac{u_T}{r} = k_1 \frac{\pi}{2} \rho_A r^3 .$$

The equation for maximum torque also can be written

$$T_{max} = \frac{1}{8} p_s \pi r^3 k_2 (1 - k_2^2)$$

where k_2 is the ratio of the outer radius to inner radius of the vanes in the orienting system.

The maximum precession rate, $\dot{\phi}_{max}$, which the system can perform is therefore

$$\dot{\phi}_{max} = \frac{T_{max}}{h} = \frac{k_2 (1 - k_2^2) p_s}{4 k_1 \rho_A v_T} .$$

Therefore, under the assumptions above, the operation of the system is completely independent of system size.

G. ORIENTATION OF THE 150 KILOWATT SPACE SOLAR POWER PLANT

The heliotropic orientation system for the 150 kilowatt space solar power consists of two sets of vanes which constitute a portion of the concentrator system described earlier. The modulating vanes are formed by dividing the outer 15 feet of the primary Fresnel reflector (between radii of 80 and 95 feet) into 180 radial strips which cause a reduced image of themselves to be directed to the outer 6.4 feet of the plane secondary reflector (between radii of 36.6 and 43 feet). This region of the secondary reflector is divided into 180 radial strips and acts as torquing vanes for the heliotropic system. The equations previously derived for maximum torque and the error angle for which it occurs are applicable with minor modification.

$$T_{max} = p_s \frac{\pi}{8} s (R_o^2 - R_i^2) \eta_g r$$

which occurs at

$$\theta_{max} \simeq \frac{\pi R_{it}}{2N\ell}$$

where p_s = solar pressure = 9.42×10^{-8} lbf/ft^2

s = normal distance from system c.g. to line connecting inner radius of torquing vane to inner radius of modulator vane = 54 ft

R_o = outer radius of modulator vanes = 95 ft

R_i = inner radius of modulator vanes = 80 ft

η_{gr} = overall reflection efficiency of primary vane

R_{it} = inner radius of torquing vane = 36.6 ft

N = number of vanes in either set

ℓ = distance between primary and secondary reflectors = 52 ft.

Evaluating T_{max} and θ_{max} gives

$$T_{max} = 0.00524 \text{ ft} \cdot \text{lbf}$$

$$\theta_{max} = 0.35^\circ \quad .$$

An operating torque of one-half the maximum torque is used which, for the precession rate required for an earth's satellite ($\dot{\phi} = 1.99 \times 10^{-7}$ rad/sec), yields

$$h = \frac{T}{\dot{\phi}} = 13,200 \frac{\text{slug} \cdot \text{ft}^2}{\text{sec}} \quad .$$

The angular momenta of the four rotational subsystems are summarized in Table III. The angular momentum of the reflector systems is chosen so as to attain the desired overall angular momentum of 13, 200 slug $\cdot$ ft^2/sec. This can be in either direction and results in two possible choices for the angular rate of the reflector system. The two possible choices are -1.726 and -1.260 rad/sec, or -0.275 and -0.20 rev/sec, respectively.

Table III Summary of Angular Momenta of 150-KW System

Item	Mass (lbm)	Radius of Gyration (ft)	Moment of Inertia ($lbm \cdot ft^2$)	Angular Rate (rev/min)	Angular Rate (rad/sec)	Angular Momentum ($slug \cdot ft^2/sec$)
Rotational Subsystem No. 1 (Boiler, Condenser, Stators)						
Condenser (dry)	326	4.3	6,030			
Gen. Cooler	105	3.5	1,287			
Torus Boiler (dry)	87	5.5	2,630			
Housing, Spokes, etc.	30	3.5	368			
Turbine & Gen. Stator	75	0.5	19			
Mercury in Boiler	48	5.5	1,452			
Mercury in Condenser	20	4.3	370			
Extensible Support Tube	50	1.0	50			
Mirror Drive Systems (2)	22	0.1	0			
TOTAL	763	---	12,206	+210	+22	+8,340
Rotational Subsystem No. 2 (Turbine and Gen. Rotors)	75	0.4	12	-11,790	-1,233	-460
Rotational Subsystem No. 3 (Reflectors, etc.)						
Primary Reflector Sys.	394	---	1,734,000			
Secondary Reflector Sys.	92	---	82,000			
TOTAL	486	---	1,816,000	-------	See Text	-------
Rotational Subsystem No. 4 (Belt System)						
Belts (due to ω)	131	---	---	---	+2.5	+40,800
Belts (due to v)		---	---	---	---	+4,000
Loading Pulleys	33	110	---	---	+2.5	+30,500
Drive System	100	4	1,600	---	+19.5	+1,000
TOTAL	264	---	---	---	---	+76,300
SYSTEM TOTAL	1,588	---	---	---	---	±13,200

V. BELT RADIATOR

A. GENERAL DISCUSSION

It has long been recognized that the major problem in building an effective, lightweight thermodynamic solar energy space power converter is that of heat rejection. This rejection must take place by radiation, unless evaporative cooling and associated mass loss can be accepted. The rejection of heat by radiation requires a radiating surface area of the same order of magnitude as the area of the solar collector unless system thermodynamic efficiency is sacrificed by using a very high rejection temperature. Since this entire area must be gas-tight and resist puncturing by micrometeoroids if a conventional condenser design is used, the condenser weight will generally be a major portion of the system weight. Further, such systems are rather complex and elaborate and are not well suited being folded into a confined space for launching. Under such conditions, little would be gained by achieving a very lightweight collector system.

Suggestions to augment radiator surface by spinning disks and belts have been made in the past by several authors (References 12 and 13). None of these, however, have appeared to be very practical, requiring either running seals for ingress and egress of the belt from the pressurized condenser or, relying upon radiative heat transfer from the condenser surface to the radiating disk. The latter, in effect, defeats the stated purpose and, in

essence, only provides some meteoroid protection without excessively detrimental radiation shielding of the basic condenser.

B. A BELT SYSTEM FOR HEAT REJECTION

A fully external belt design, rotating on the condenser has been conceived that shows promise of overcoming the problems discussed above. The belt is in physical contact with the condenser and, because of its relative motion, continually removes the heated contacting portion away to the free loop portion. During the period required by the belt to return to the condenser, heat will be radiated off both surfaces such that the belt returns to the condenser at considerably lower temperature. Note that the belt has essentially only rolling contact and has no substantial gliding friction with the condenser surface. A balanced configuration employing three belt loops spread 120° providing low mutual irradiation is shown in Figures 25 and 26. Other possible configurations include two-belt systems and twisted belt geometries.

A drive system will be required to compensate for the rolling friction between the condenser can and the belt and for the hysteresis losses in the belt as it is flexed. Unless such energy losses are made up by applying a torque between the can and belts, the belt system will eventually have the same angular velocity as the can and will not roll at all. The drive system should, in addition to making up for friction losses, also preserve symmetry of the belt system.

The immediate drive of the belts might be by rollers, electrostatic

forces, electromagnetic forces, or others. However, to obtain the desired belt-system angular velocity, a synchronous drive system will be required which can position the devices which drive the belts. A system of rollers is shown schematically in Figure 27.

C. ANALYSIS OF BELT SHAPE AND TENSION

A belt system has been analyzed where a perfectly flexible belt goes around a central rotating pulley with a fixed axis (as the condenser can will essentially be with a balanced system of belts moving on it) and travels around a belt-tensioning pulley as shown in Figure 28. The geometry of the problem is assumed to be of fixed shape but rotating at the velocity, ω, about the central pulley. Every point on the belt and the periphery of each pulley is moving at the velocity, v, with respect to the revolving geometry of the problem.

Let m' = mass of belt per unit of length

v = velocity of belt with respect to revolving geometry

r = radius to point P

r_o = radius of central pulley

β = angle between pulley and radius at point P

ρ = radius of curvature of belt at point P

ω = angular velocity of fixed shape of pulley

T = belt tension at point P

T_o = belt tension at $r = r_o$.

The analysis shows that

$$T = T_o - \frac{m' \omega^2 (r^2 - r_o^2)}{2}$$

and

$$\rho = \frac{\left[\left(\frac{T_o}{m' v^2} - 1 \right) - \frac{\omega^2 r^2}{2 v^2} + \frac{\omega^2 r_o^2}{2 v^2} \right]}{\left[\frac{\omega^2 r^2}{v^2} \sin\beta + \frac{2 \omega r}{v} \right]}$$

where the radius of curvature is given as a function of r and β . The shape of the belt can quite readily be laid out using simple computation and a compass. If it is desired to compute and display a range of solutions, the above equation can be written in terms of dimensionless groups as

$$\rho' = \frac{b - \frac{a^2}{2} (r'^2 - 1)}{a (a r' \sin\beta + 2)}$$

where

$$a = \omega r_o / v$$

$$b = T_o / m' v^2 - 1$$

$$r' = r / r_o$$

$$\rho' = \rho / r_o \quad .$$

Thus, the shape of the curve can be obtained for a desired combination of a and b corresponding to a particular set of speeds and upon the desired belt tension (or normal pressure) at the condenser can. Since the solution is symmetrical with respect to some center line, only one branch of the curve need be constructed. If it is desired to terminate the belt system at a smaller radius than the one obtained in the above manner, it can be accomplished by means of a belt-tensioning pulley, the mass of the pulley being such that its centrifugal acceleration can furnish the specified tension to the belt at the first point of contact between belt and pulley.

Belt shapes have been computed for several sets of conditions and

two of these are shown in Figure 29. The large loop in either case can, if desired, be eliminated by the use of a loading pulley at a radius somewhat less than the maximum shown. It is of interest to note how the so-called Coriolis force causes a different form of curvature in the two cases shown.

D A BELT RADIATOR FOR THE 150-KW SPACE SOLAR POWER SUPPLY

A preliminary analysis of the belt radiator system for the 150-KW system has lead to a design where the belt is of 0.006 inch fiber reinforced TFE ("Armalon") and terminated on a loading pulley that has its center at a radius of 110 feet from the condenser axis. The belt system rotates in the same direction as the condenser. Also:

r_c = 4.2 feet (average)

ω_o = 22 rad/sec

r_{max} = 110 feet

$\sigma(r_o)$ = belt tensile stress at condenser = 1000 lbf/in^2

ρ = density of belt material = 2.7 $slug/ft^3$

ω = 2.5 rad/sec

$v = r_o(\omega_o - \omega)$ = 82 ft/sec

$a = \omega/\omega_o - \omega$ = 0.128

$b = \left(\sigma_o/\rho v^2\right) - 1$ = 6.96 .

The average belt is 250 feet long and the total width of belts is 12 feet (allowing a total of one foot for spacing between belts). The resulting weights are:

M_b = mass of belts = 4.05 slug = 131 lbm

M_p = mass of loading pulleys = 33 lbm .

The various anguiar moments are then:

h_{b_ω} = angular momentum of belts caused by rotation

= 40, 800 slug·ft^2/sec

h_{b_v} = angular momentum of belts caused by velocity, v

= 4000 slug·ft^2/sec

h_p = angular momentum of loading pulleys

= 30, 500 slug·ft^2/sec .

E. HEAT TRANSFER BETWEEN BELT AND CONDENSER

The utility of the proposed belt radiator will depend largely upon the mechanism of heat transfer from the condenser surface to the belt, in hard vacuum. Mechanisms of heat transfer, that can be postulated are:

- Radiation in areas of gaps between condenser and belt surface
- Conduction in areas of solid or liquid contact
- Convective transfer due to evaporation and condensation of belt and condenser material in the volume formed by the intervening gaps .

Clearly, the conductive and convective transfer needs to be a substantial portion of the total heat transferred, in order to obtain a benefit from the belt. It is also clear that both will strongly depend upon the materials selected for condenser surface and belt, and on the contact pressure between the two surfaces, which is generated by the rotational motion of the belt.

In order to obtain some preliminary data on expected heat-transfer an experimental set-up shown in Figure 30 was used. It consists of a heated

drum supporting a weighted idler roller through a flat belt. Both, drum and idler are provided with a crown to prevent run-off of the belt. The crown also provides a slight amount of sliding motion between belt and drum which is believed to increase the heat transfer between the two surfaces. Temperatures are measured in the drum and idler and in the two branches of the belt. The drum can be rotated at variable speeds by a gear drive.

The whole assembly is placed into a vacuum bell jar connecting to a diffusion pumping system. The pumping system is capable of maintaining a pressure of approximately 2×10^{-6} torr with the heated and running assembly in the bell jar.

The experiment consists in establishing the electrical power required to maintain the drum at a fixed temperature at various belt speeds. The excess power consumed by the heater to maintain constant drum temperature for a running belt yields a measure for the heat transported by the belt.

The experiment was performed first over a range of belt speeds at constant vacuum. Typical results shown in Figure 31 indicate that at speeds above 3 in/sec (corresponding to less than approximately 1 sec dwelling time of belt at drum surface) the convective cooling capability of the belt is saturated.

A second series of experiments then was performed, in which the bell jar pressure is varied from approximately 1mm Hg to 10^{-6} mm Hg (the capacity of the vacuum system employed). At each level, the pressure is

maintained until thermal equilibrium is established by both standing and running belt. The difference in required heating power is again interpreted as heat transported by the belt. Figure 32 shows a typical set of data, indicating that at ambient pressures below 10^{-2} mm Hg, the effect of pressure begins to vanish. From these data it can be concluded that the heat transfer of the belt measured at 2×10^{-6} mm Hg should be reasonably representative for its performance in a hard space vacuum.

Several belt materials (shown in Figure 33) have been tested including TFE film, woven TFE fiber and woven graphite cloth. All belts performed satisfactorily for total running times of several hundred hours with the exception of a knitted carbon fiber cloth belt that showed serious mechanical damage after several hours.

An analysis of the data shows, that under the conditions tested, heat loss of the drum is increased by the belt by a factor of approximately 2.5 over that experienced by radiation alone. Thus, condenser surfaces can be reduced significantly below those required for simple radiators.

Considerable additional experimental work will be required to develop realistic and quantitative design criteria and guides for optimum belt materials selection for the condenser surface temperature range that is of interest. A basic research program, directed at obtaining a fundamental understanding of the heat transfer mechanisms between contacting and sliding surfaces in vacua will be required to provide the necessary guides for this development.

A GENERAL DESCRIPTION

The Huettner turbine is a closed cycle steam engine that has been proposed for automotive and auxiliary power applications as early as 1934 (References 14, 15, 16, 17). It consists of a rotary boiler-condenser system of such a geometry that boiler pressure is generated directly by centrifugal forces. This eliminates the necessity for auxiliary condensate feed pumps, improves heat transfer, and improves vapor-liquid separation in both boiler and condenser. It also provides an extremely compact and potentially light-weight configuration. These features are most significant for space applications.

One of the principal difficulties of operating a steam engine in free orbit is the absence of gravity, which causes severe and well-known operational difficulties with conventional configurations. The extremely high artificial gravity provided by the Huettner configuration does two significant things.

a) It drastically improves free convective solid-to-liquid heat transfer rates, due to the high Grashoff numbers achieved

b) It eliminates altogether difficulties with "zero g" vapor-liquid separation, which is particularly troublesome in conventional, stationary condensers and boilers.

The Huettner principle has been adapted for a space power plant by several modifications to the originally published concepts. A configuration of this adaptation to a solar mercury turbine is shown in the schematic of Figure 34. Details of the central mechanism are shown in Figure 35.

The complete "static" assembly of boiler, turbine-alternator casings and condenser must be visualized as rotating at moderate speed in free inertial space. The twin radial turbine wheels and the alternator armature are mounted on a common short shaft, counter-rotating the "static" assembly at high speed.

The boiler has the form of a toroidal ring and is pressurized by the liquid mercury column in the condensate feed line, leading from the condenser to the boiler. Heat input to the boiler surface causes mercury vapor generation at high pressure.

Vapor is superheated by choking the flow from the boiler through the vapor feed into the central inlet manifold at the end of the turbine stator assembly. This method of superheating avoids the necessity of large additional susceptor surfaces for heat transfer to vapor at poor transfer coefficients. Thus, it also materially reduces weight and re-radiation losses associated with conventional superheaters.

The superheated vapor is expanded through the twin radial outflow stages of the turbine into the outlet manifold. From there, it is fed to the radiating conical condenser assembly where the exhaust vapor is condensed. The resulting condensate is driven by the centrifugal force along the inclined

condenser surface radially outward towards the condensate feed line, where the working fluid re-enters the thermodynamic cycle.

Several additional features of the turbo-alternator assembly are also shown in Figure 14 which relate to the pressurization and cooling of the alternator, and to the details of the shaft bearing portions of the design.

The turbine is two-sided which eliminates net axial thrust forces on the shaft and reduces bearing forces to those unavoidably generated by rotary unbalance and precessional motions. This is considered an extremely important feature in alleviating currently experienced serious bearing problems in liquid metal Rankine cycle space power plants.

Since the power plant is intended for long-term operation, leakage of working fluid to the space-vacuum will be unacceptable. Thus, to avoid rotary seals, the alternator assembly is encased into a pressure-tight enclosure which is integral with the rotating turbine case. This alternator casing is pressurized by helium (or other inert gas) to a pressure equal to that in the turbine outlet manifold.

Inert-gas pressurization of the alternator case accomplishes three purposes:

a) The windage losses of the high-speed alternator rotor are reduced to negligible amounts

b) Leakage of working fluid through shaft labyrinth seals placed between turbine and alternator are due only to diffusion since no pressure differential is allowed to exist, and

c) Heat conducted by the shaft and generated in the alternator is effectively removed by convection and carried to the alternator-cooling radiator. This permits the bearings and alternator assembly to operate at tolerable temperature despite the relatively high condensate temperatures required for an efficient radiating condenser.

Since the alternator case will be cooled to a temperature considerably below that of the condenser, diffusing working fluid will immediately condense and only the amount corresponding to the small partial pressure of the condensate will remain in vapor form in the alternator case. Condensed fluid will be re-supplied to the thermodynamic cycle through the leakage condensate feed tube connecting alternator casing and boiler.

The choice of the features of this cycle are derived from several detailed studies and reference surveys that have been conducted in support of this preliminary design. No attempt has been made to optimize the overall system. Sufficient engineering data has been generated, however, to allow what is believed to be a conservative estimate of the thermodynamic and mechanical performance of the proposed system, and to identify the principal development problems that remain to be resolved in a future program. Results of these studies and reasons for the particular design choices made are summarized in the subsequent paragraphs.

B. THERMODYNAMIC CYCLE

Figure 36 shows the upper portion of two different Rankine cycles

in the enthalpy-entropy diagram for mercury (Reference 18). The dashed line gives a conventional Rankine cycle with vaporization to the saturation point, reached at 930°F, and then on to a super-heated state at 1160°F, which is selected to give 6.5% moisture content at the end of the expansion in the turbine.

The enthalpy increase through the superheating phase from 930°F to 1150°F creates severe problems for the mirror-boiler system requiring a superheater surface area 2.5 times larger than that required for the boiler. This is due to the relatively poor heat transfer between superheater wall and vapor. Therefore, an unusual superheating system, shown with the solid line of Figure 36, was selected. Here, all heat addition is accomplished in the liquid phase, and under saturation conditions at a pressure of 300 psi (compared to 115 psi for the conventional heating). No heat at all is added during the superheating process. Instead, the superheating is accomplished through use of the Thompson-Joule effect, by workless throttling from 300 psi to 115 psi, which also raises the temperature from 1097°F to 1150°F because of the deviation of mercury vapor from an ideal gas.

The disadvantage of this system is an increase of the liquid-pumping work, the increase in structural weight in the boiler due to the higher working pressure, and the higher boiler temperature. The pumping work is almost negligible, (1.15 K joule/Kg) and the boiler weight is only a small fraction (less than 3%) of the total weight even for the 300 psi pressure level selected for the cycle. Further, a detailed study for the small-diameter, multiple-tube boilers selected for the two systems considered shows that boiler-

wall thickness is determined by minimum-gage considerations rather than by strength. Finally, the advantage of lower boiler temperature in the conventional superheat system is lost because of the large superheater area required, operating at temperatures well above the 1120° F used in the selected choke system.

C. BOILER DESIGN

Figure 37 summarizes information on nucleate boiling of mercury, taken from Reference 19. These data apply to a gravitational field of 1 g for which experimental data are available: The centrifugal acceleration provided by the rotating torus boiler will tend to yield still higher heat flux densities (Reference 20). The chosen heat-flux density through the boiler wall of $320 \frac{kw}{m^2}$ for a 12° C temperature drop from wall to boiling mercury is, therefore, a conservative value.

A study was conducted relative to the choice of boiler-tube diameters. For large-diameter tubes, the weight of mercury contained in the boiler becomes prohibitive. A tube diameter of 1.375" O. D. was selected as near optimum from the standpoint of weight, surface area and fluid flow characteristics. Four liquid-feed inlets and four vapor outlets, spaced by 45°, are employed. The study shows that vapor velocities in the boiler are tolerable and that liquid-level variations due to "welling" at the liquid inlets are small compared to the selected tube diameter. The vapor-outlet spokes are small in diameter to provide the desired choking for superheat. The spoke inside diameter required for this purpose is 0.125" for the 28 spokes

used in the 15 KW design. Boiler and vapor-feed tubes are made from high-temperature-resistant alloy ("Rene 41" or equivalent) coated at the inside with tantalum for protection against corrosion and leaching by the boiling mercury.

The individual boiler tubes are spaced from each other by attached fins to provide the required absorber area. A study of optimum fin geometry has been made including consideration of temperature variations along the fin span. Beryllium has been selected as fin material due to its low weight and high thermal conductivity.

D. THE MERCURY TURBINE, ITS BEARINGS, SEALS AND GENERATOR COOLING

A radial-outflow turbine with three stages, as shown in Figure 35, is proposed. It appears that a radial-outflow design, gives the best possibility of maintaining the narrow clearances demanded by a turbine of small output, since only diameters and not axial locations have to be held to close tolerances.

Furthermore, a multi-stage axial turbine would demand bearings on both turbine ends. Since the condensate temperature is 620° F, the bearing design on the condenser side (inside a hot mercury atmosphere) would represent a difficult problem. The radial-outflow turbine, on the other hand, makes cantilevered bearing arrangements easily possible. Here the bearings can be placed at some distance from the turbine and in contact with the cooled generator housing.

The high-pressure, high-temperature vapor inlet is routed in such

a way that no high-pressure seal is necessary; the feeder tubes lead into an all-enclosed central plenum. The design also incorporates a feature which makes a low-pressure seal between the generator and turbine housing unnecessary.

The sealing and bearing problem is coupled with the problem of cooling the generator and its bearings. The generator is cooled to 300° F by a separate cooling radiator.

Unless a seal between the 620° F turbine-condenser space and the 300° F generator space is provided, the mercury enters the generator through the bearing. In the generator, a vacuum will be formed, since the mercury condenses (maintaining only the .08 psi saturation pressure at 300° F). This condensate is thrown to the periphery of the revolving generator housing and is then pumped back centrifugally to the condenser, by way of the mercury return pipes.

In order to minimize this mercury pumping cycle through the generator without resorting to the use of seals, it is proposed to fill the entire combined space of condenser, turbine housing and generator housing with helium, in a quantity which gives 8.5 psi total pressure at the 620° F condenser operating temperature. This results in a partial-pressure distribution between mercury vapor and helium which varies according to the different container temperatures. In the condenser, the mercury partial pressure will be 8 psi and the helium partial pressure 0.5 psi. In the 300° F generator housing, the mercury partial pressure will be only 0.08 psi, while the helium partial

pressure now amounts to 8.42 psi.

The combined pressures amounting to a total of 8.5 psi in each of both containers now maintain a balance between the two containers. Mercury inflow into the alternator casing will take place only through diffusion. This diffusion can be held at a minimum by means of a simple labyrinth. The excess vapor which enters through this labyrinth will immediately be condensed (since it is in excess of the partial pressure at the saturation point) and trickle back to the revolving generator periphery and from there via the return line to the boiler. Only if the partial pressure of mercury in the condenser exceeds 8.5 psi, (for instance, because of insufficient condenser cooling) will mercury vapor be pumped into the generator. Consequently, the margin of partial pressure of helium has to be sufficient to avoid this contingency. (The margin of 0.5 psi given in this example may be insufficient. Only by means of a future study on the regulation of this turbine system can the necessary margin be determined.)

Besides the advantage of preventing mercury entry into the bearings and generator the helium filling offers three more advantages.

1. The first advantage relates again to the generator cooling the helium atmosphere serves to transfer all generator heat to the cooling cone, which is dimensioned to reject all generator heat by radiation at 300° F
2. The helium atmosphere cuts the windage losses in the generator to a low level. (Calculations show that a generator initially considered as operating inside the condenser cone with a mercury-

vapor atmosphere of 8 psi would suffer from excessive windage losses)

3. On the launching pad, and while traversing the atmosphere, a filling gas is necessary. The outside pressure would otherwise collapse the thin shell of the condenser tubing.

It is, therefore, proposed to initially fill the entire system with helium to a pressure of 15 psi. The excess helium will blow off through a regulating valve during first stage flight until 8.5 psi at proper operating temperature is reached.

VII. CONCLUSIONS

Figure 38 shows a comparison of specific power data for several currently proposed or developed space power generating systems taken from Reference 21. It appears that for the power range covered by the present study, the proposed rotating deployable solar power system is markedly superior to alternatives. Thus, a re-evaluation of the relative merits of the various approaches to space power generation would appear to be in order.

Before the proposed concepts can be seriously considered for incorporation into a practical system, several areas will require further study and development, as outlined below.

- Experimental research program, directed towards an understanding of the heat transfer phenomena of contact surfaces in vacuum, and development of satisfactory belt and interface materials.
- Theoretical and experimental study of the dynamics of the proposed belt system, both during deployment and during steady state. This study should include the out-of-plane motions of the belt and account for non-planar (i. e. twisted) belt arrangements.
- Experimental prototype design and test evaluation of the proposed rotary Rankine cycle turbine system (Huettner turbine).

- Fabrication and testing of full scale net-supported Fresnel surfaces.
- Experimental verification of the performance characteristics for the proposed heliotropic orientation system using radiation pressure. Such a program should culminate in the launching, orbital deployment, tracking and data telemetry of a moderate sized spinning reflector assembly.

With the data obtained from these programs, a systems optimization study can be conducted. For the purpose of an initial feasibility demonstration, it would be desirable to fix the power output of such an optimized system at approximately the 15 KW level.

This optimized system, then, should be developed and subject to evaluation in orbital flight.

REFERENCES

1. McClelland, D. H., and Stephens, C. W., "Energy Conversion Systems Reference Handbook," Vol. II, Electro-Optical Systems, Inc., EOS Rpt 390-Final, WADD Tech Rpt 60-699, Sept. 1960.

2. Heath, Atwood R., Jr., "Status of Solar Energy Collector Technology," in "Power Systems for Space Flight-Progress in Astronautics and Aeronautics - Vol. II," Academic Press (1963).

3. Lyman, Robert and Houmard, James E., "Inflatable Foam-Rigidized Approach to Solar Concentrators," in "Power Systems for Space Flight-Progress in Astronautics and Aeronautics - Vol. II," Academic Press (1963).

4. Tyler, R. D. and McClure, R. B., "Materials and Construction Techniques for Space Solar Reflectors," in "Power Systems for Space Flight-Progress in Astronautics and Aeronautics - Vol. II," Academic Press (1963).

5. Lin, B. Y. H., and Jordan, R. C., "Performance and Evaluation of Concentrating Solar Collectors for Power Generation," ASME Paper No. 63-WA-114.

6. "Sunflower Solar Collector," Thompson Ramo-Wooldridge. Inc., NASA CR-46, May 1964.

7. Kyser, A. C., "Uniform-Stress Spinning Filamentary Disk," Astro Research Corporation, ARC-R-150, May 29, 1964.

8. Schuerch, H., "Structural Analysis of ECHO II," Final Report, Astro Research Corporation, ARC-R-116, October 23, 1963.

9. Frye, W. E., and Stearns, E. V. V., "Stabilization and Attitude Control of Satellite Vehicles," ARS Journal, December 1959, p. 927.

10. Smythe, W. R., "Static and Dynamic Electricity," McGraw-Hill (1939).

11. Ule, Louis A., "Orientation of Spinning Satellites by Radiation Pressure," AIAA Journal, July 1963, pp. 1575-1578.

12. Weatherston, R. C., Smith, W. E., "A New Type of Thermal Radiator for Space Vehicles," IAS Paper No. 60-78, June 1960.

13. Weatherston, R. C., "The Radiation Amplifier - A New Approach to Heat Rejection from Space Power Plants," IAS Paper No. 62-73, January 1962.

14. Ostwald, W., "Die Huettner - Dampfturbine," ATZ 37, 22, November 25, 1934.

15. Muenzinger, F., "Neue Wege zu billiger Spitzenkraft," Electrotechn. Zeitschr, 1934, 12, March 22, 1934.

16. Huettner, F., "Die Huettner Turbine," Elektrotechnische Zeitschrift, 1934, Heft 30, p. 742-744.

17. Stodola, A., "Der Sulzer-Einrohr-Dampferzeuger," ZVD, Vol. 77, p. 1225-1232, 1933.

18. Perry, R. H., "Chemical Engineer's Handbook," 4th ed., McGraw-Hill, 1963.

19. Engelberg, Forster, K., Greif, R., "Heat Transfer to a Boiling Liquid - Mechanism and Correlations," Trans. ASME 81, p. 51, 1959.

20. Graham, R. W., Hendricks, R. C., "A Study of the Effect of Multi-g Accelerations on Nucleate Boiling Ebullition," NASA TN D-1196, May 1963.

21. Menetry, W. R. and Fisher, J. H., "Energy Conversion Systems Reference Handbook," Vol. I, Electro-Optical Systems, Inc., EOS Rpt 390-Final, WADD Tech Rpt 60-699, Sept. 1960.

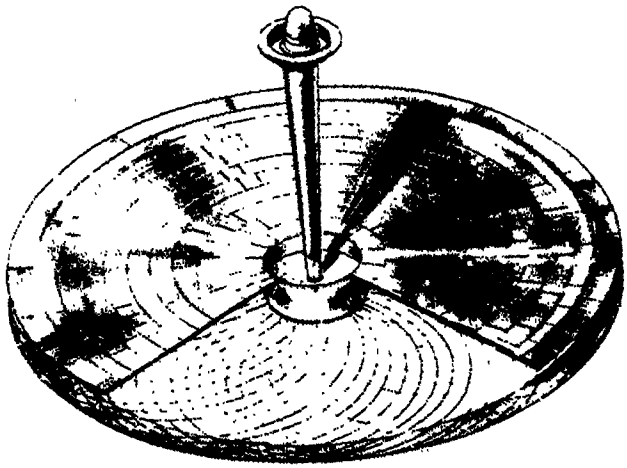

Figure 1. 15-Kilowatt Space Solar Power Supply

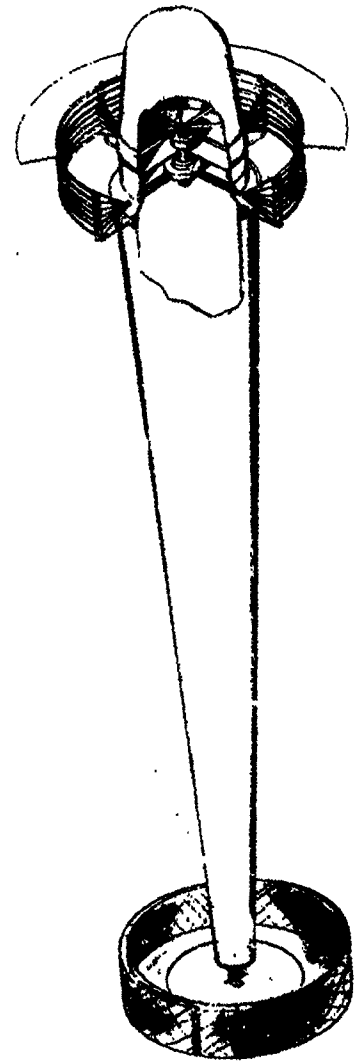

Figure 2. 15-Kilowatt System Folded

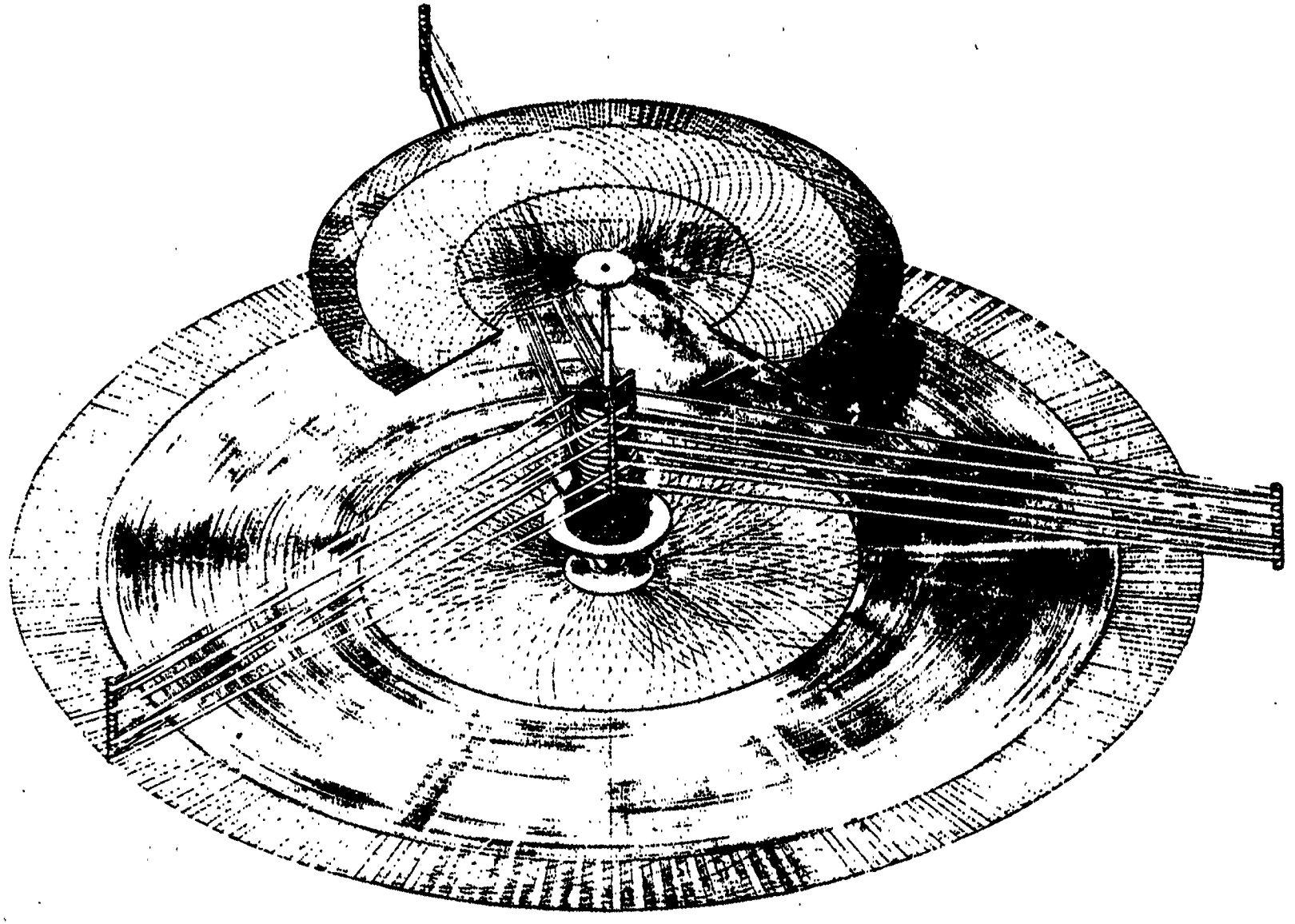

Figure 3. 150-Kilowatt System Deployed

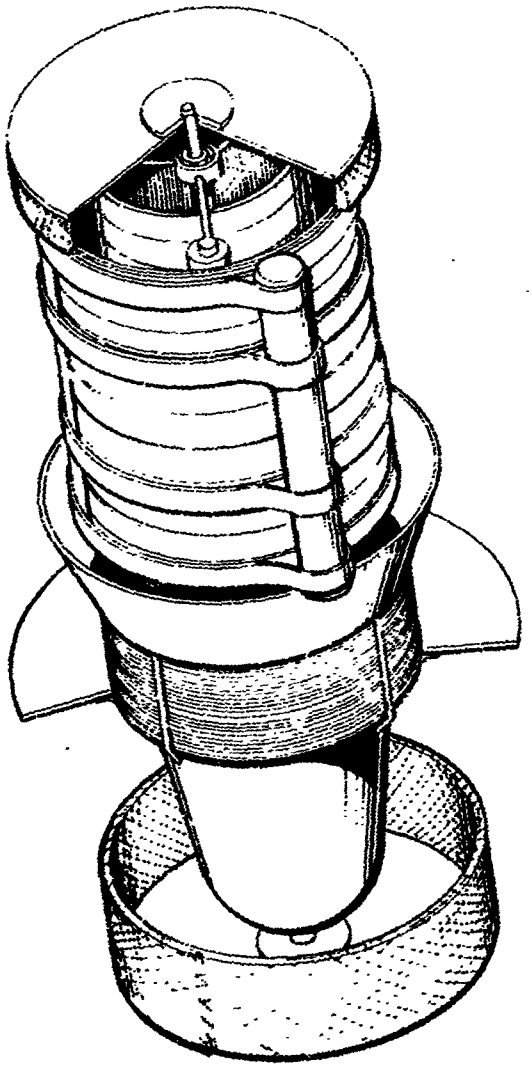

Figure 4. 150-Kilowatt System Folded

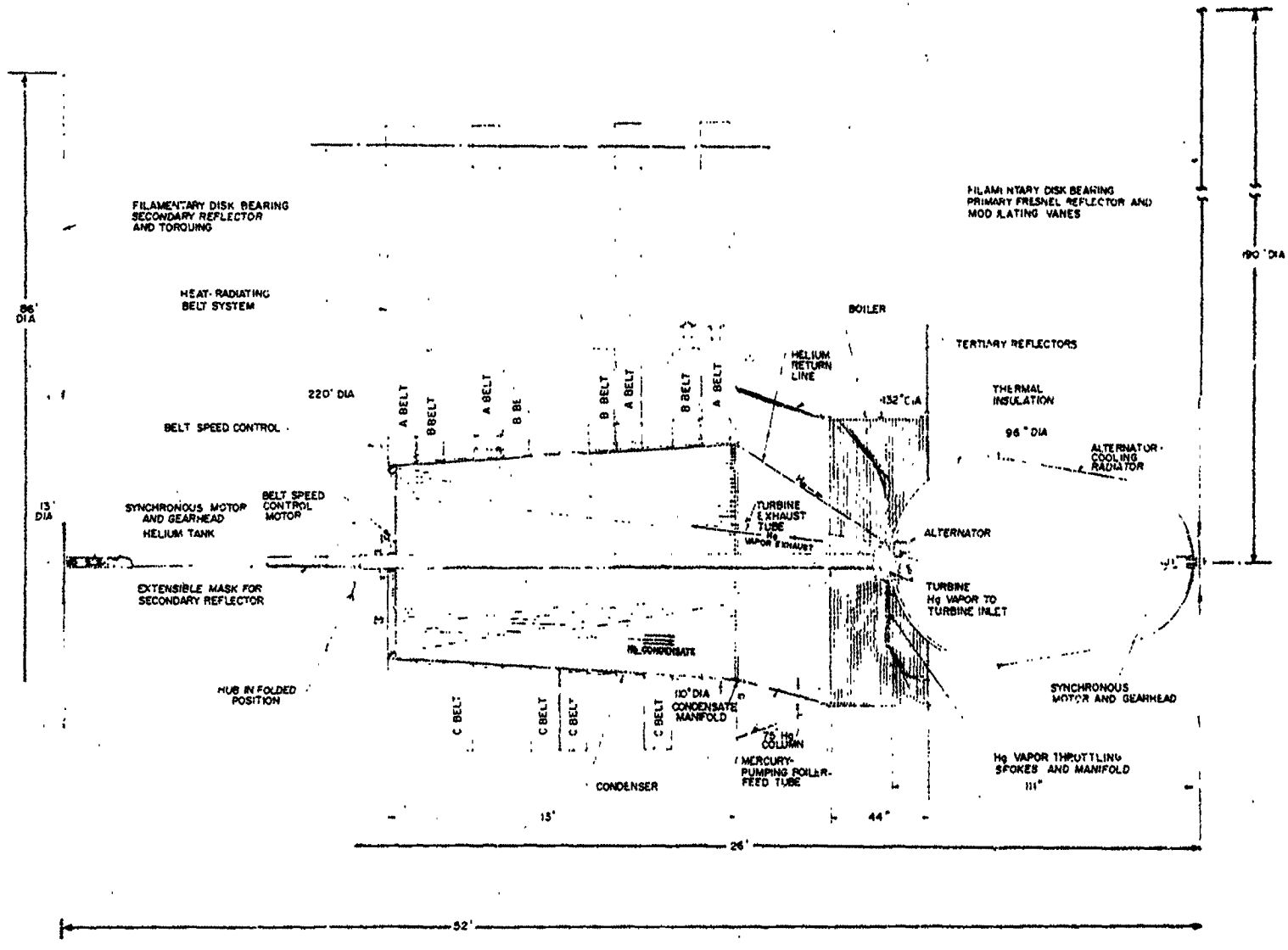

Figure 5. Details of 150-Kilowatt System

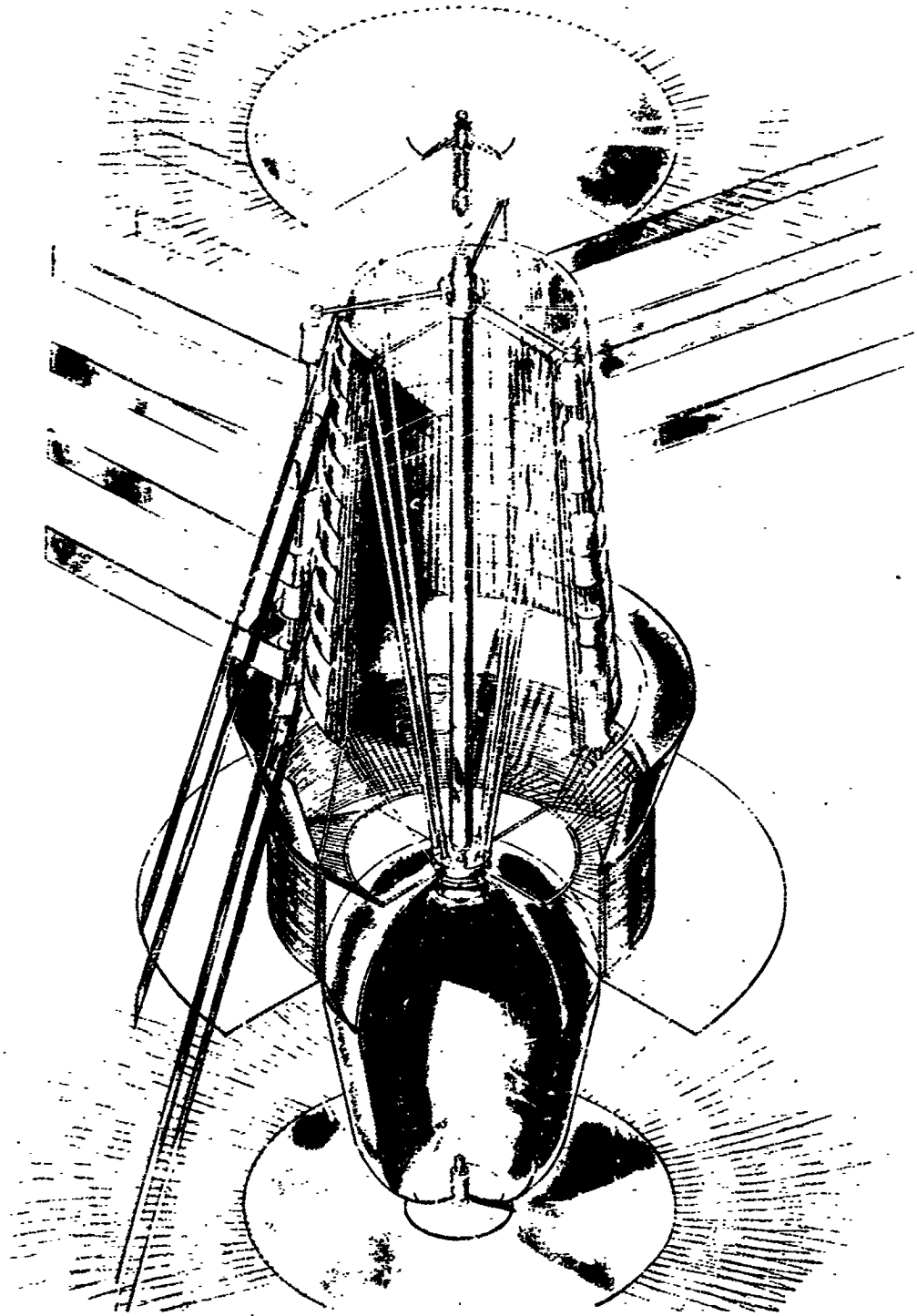

Figure 6. Central Mechanism of 150-Kilowatt System

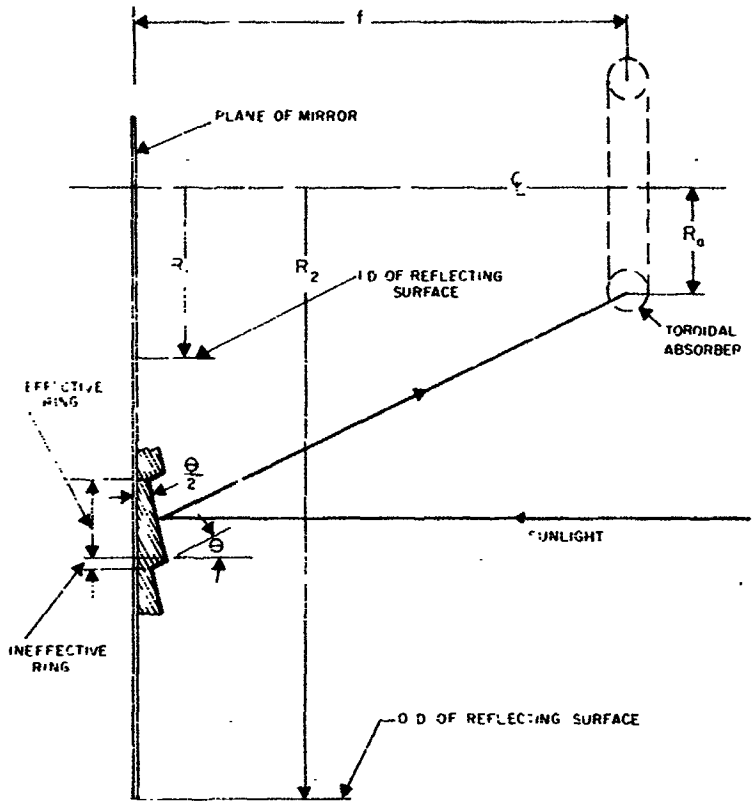

Figure 7. Schematic Cross Section of Fresnel Reflector

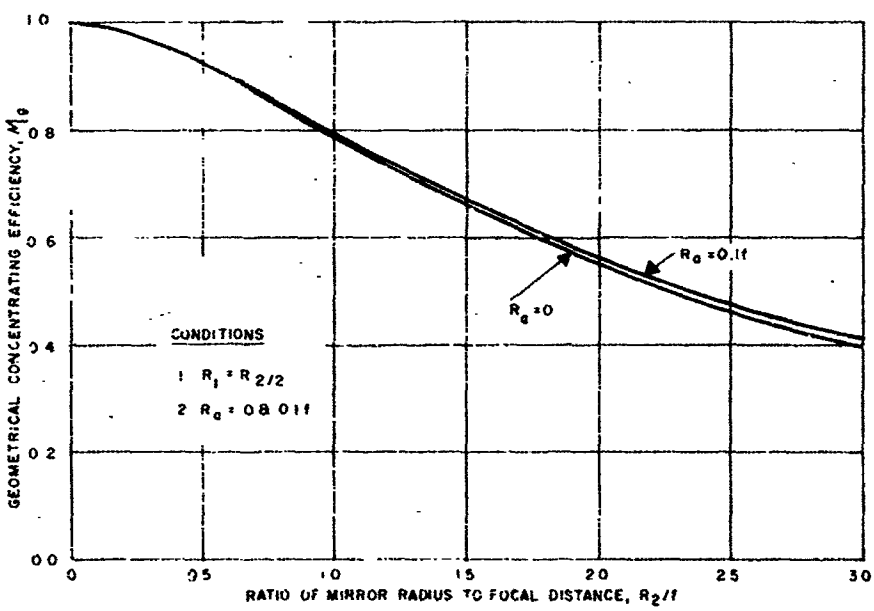

Figure 8. Geometrical Concentrating Efficiency

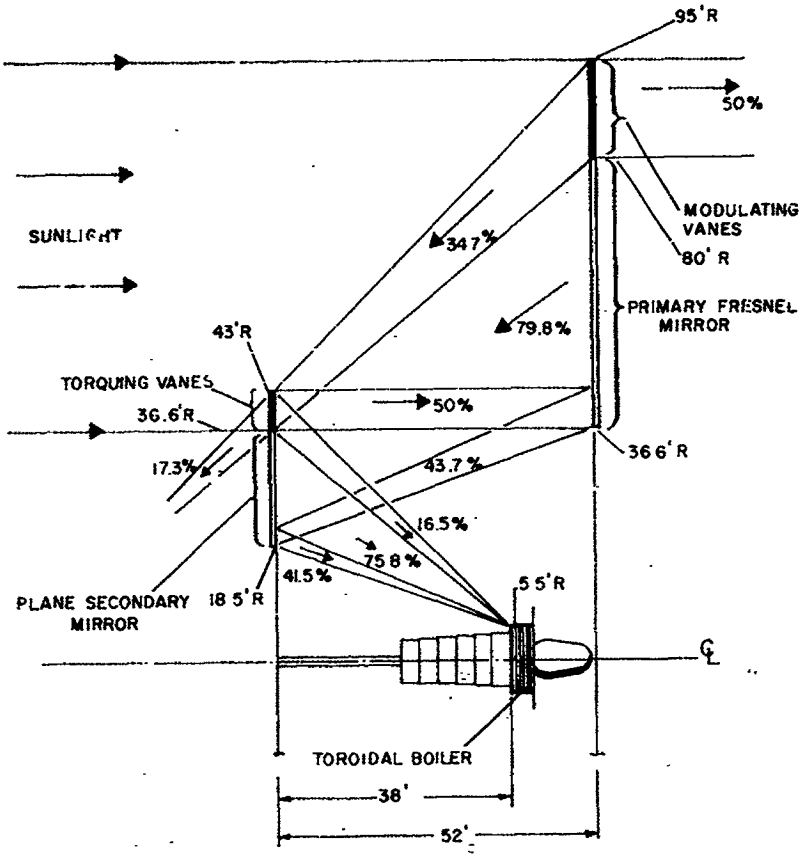

Figure 9. Reflector System for 150-Kilowatt Power Supply

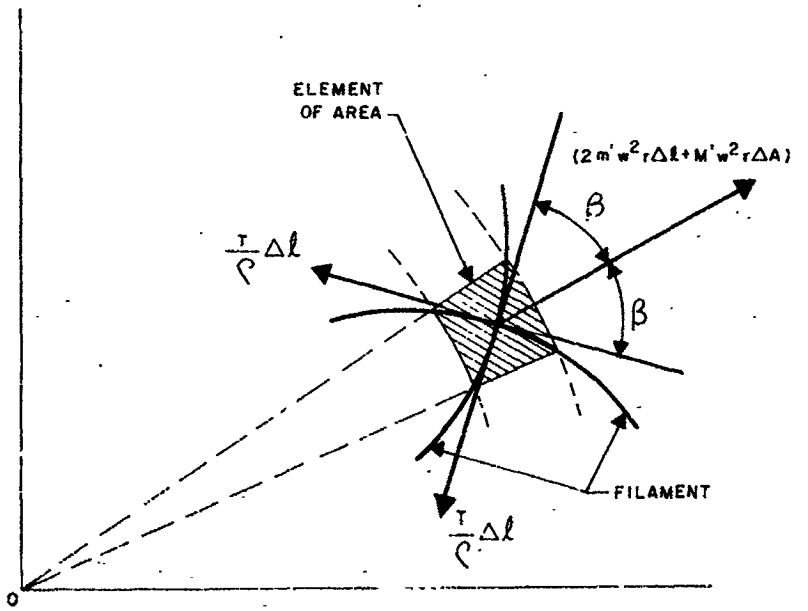

Figure 10. Forces on Net Element

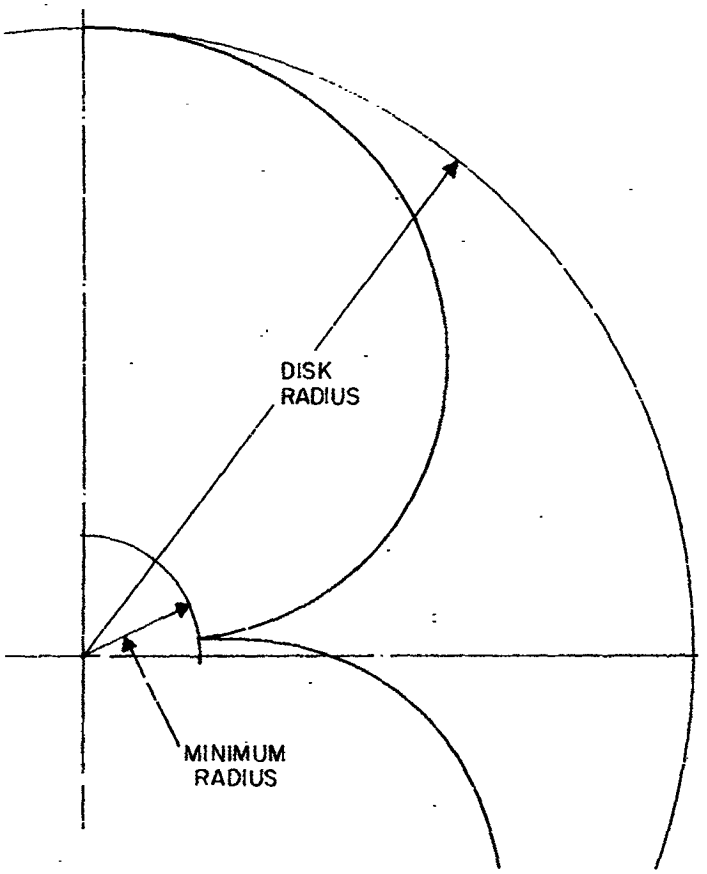

Figure 11. Net Geometry for $\mu = 1$, $\Omega = \frac{3}{2}$

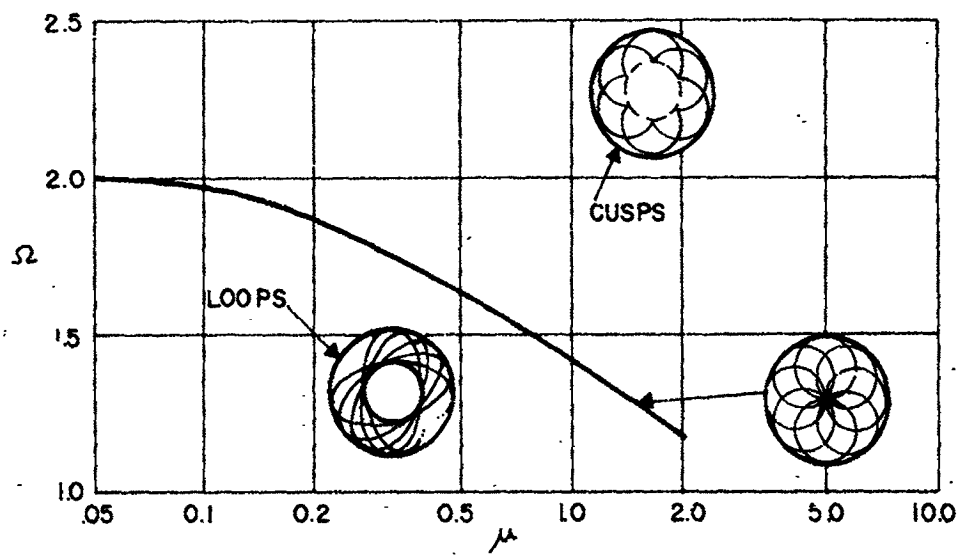

Figure 12. Domain of Solutions in $\mu - \Omega$ Plane

Figure 13. Focusing of Sunlight by Thin Fresnel Reflector

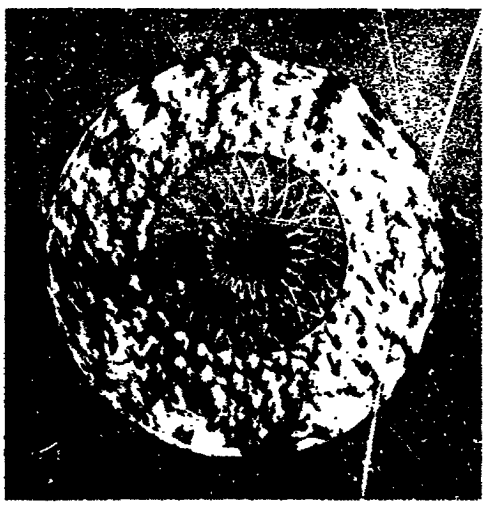

Figure 14. Annular Mirror Expanded

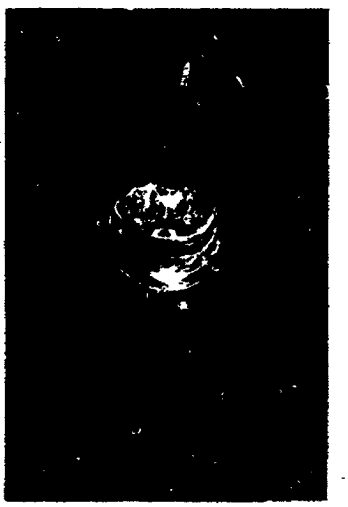

Figure 15. Annular Mirror Folded

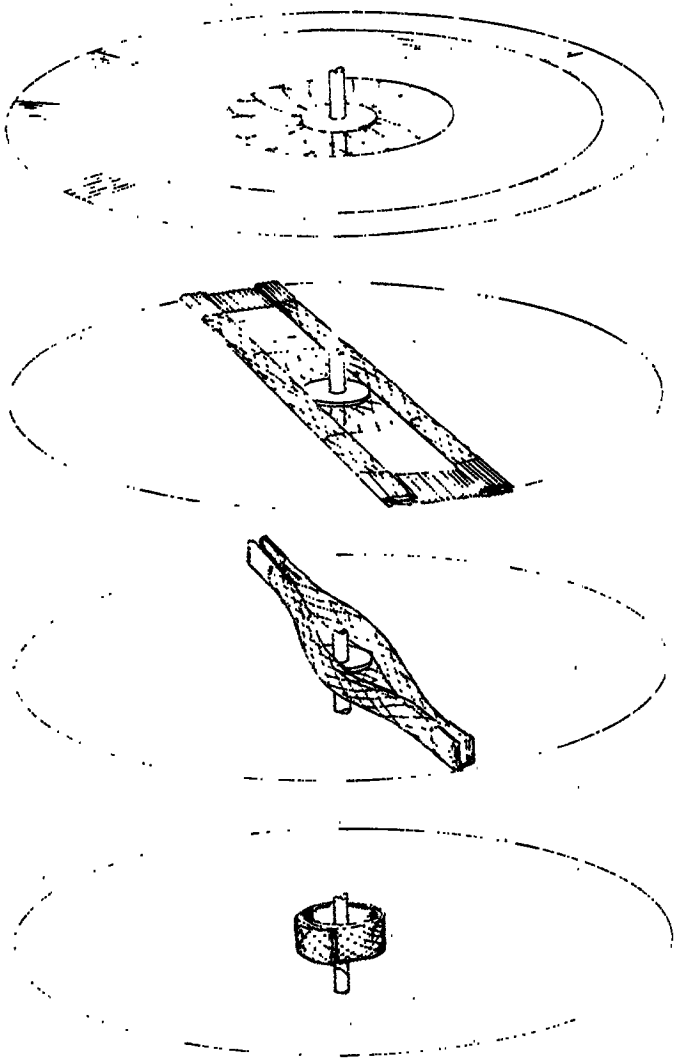

Figure 16. Folding of Reflector into Toroidal Package

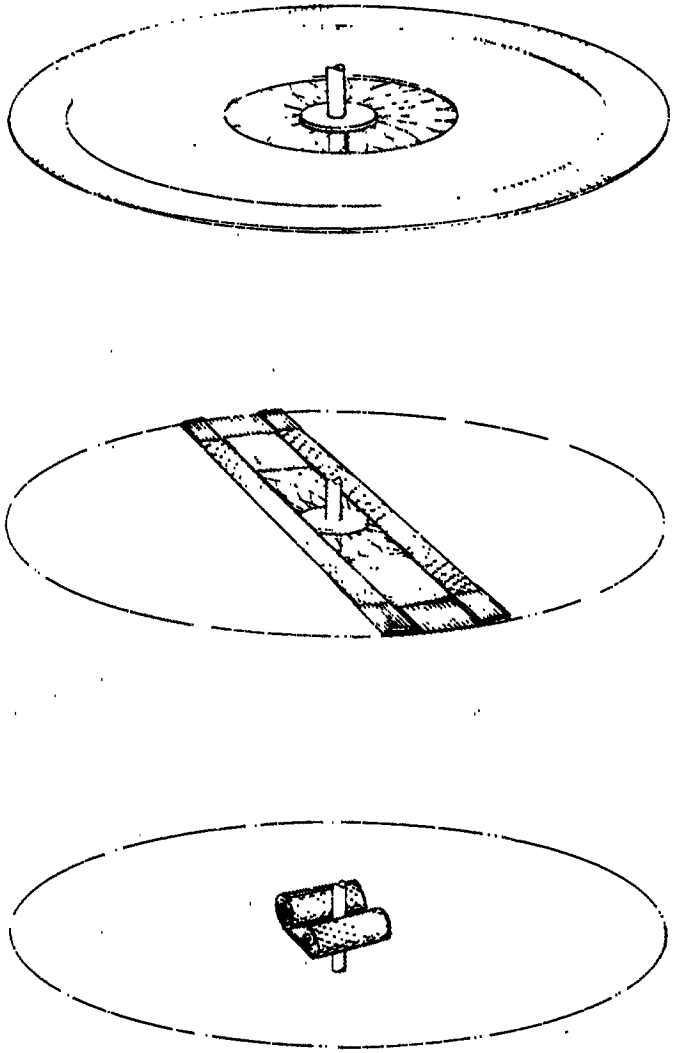

Figure 17. Folding of Reflector into Double Roll

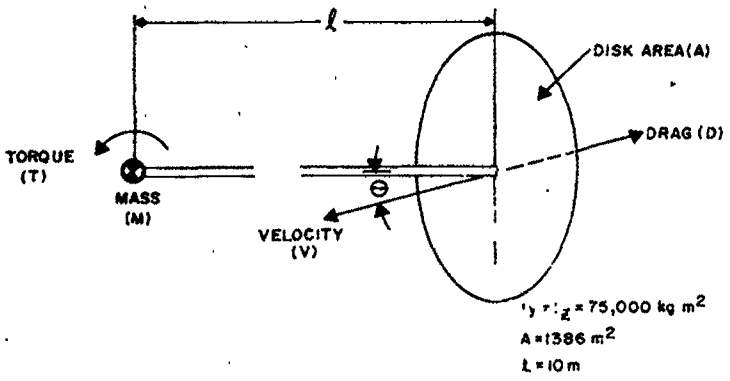

Figure 18. Geometry of Aerodynamic Forces on System

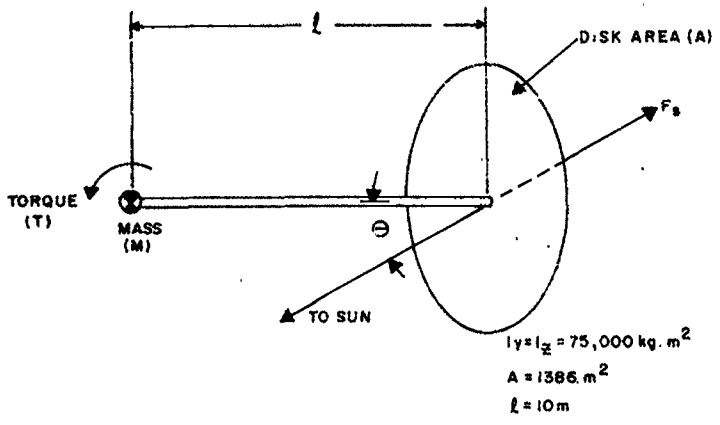

Figure 19. Geometry of Solar Pressure on System

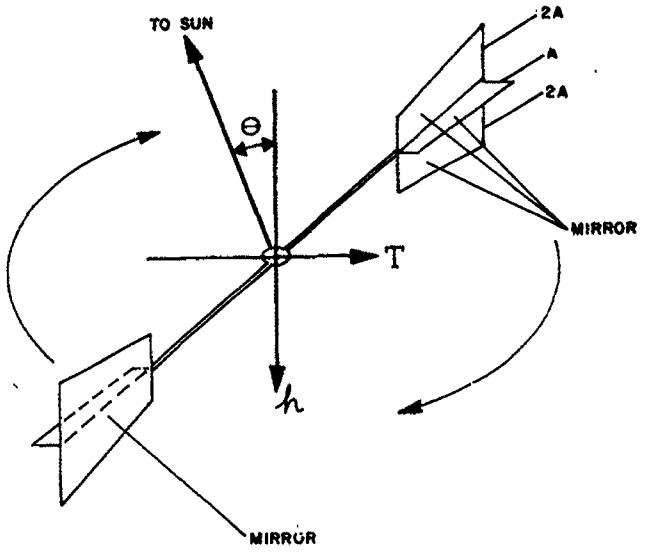

Figure 20. Heliotropic Orientation System of Ule

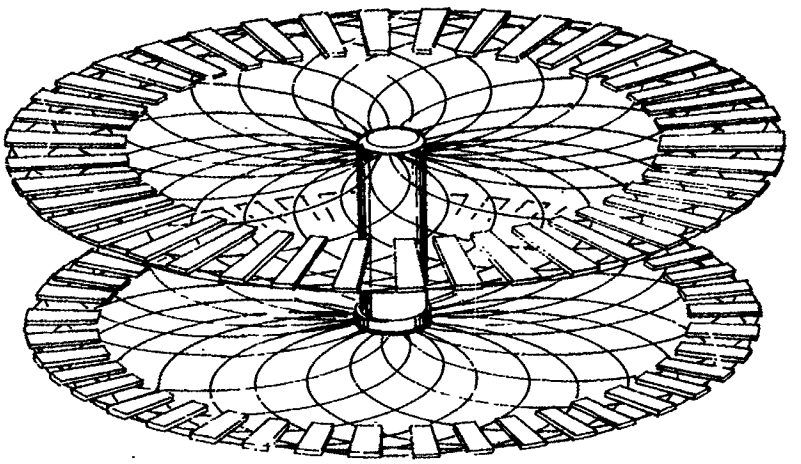

Figure 21. Overall View of Heliotropic System

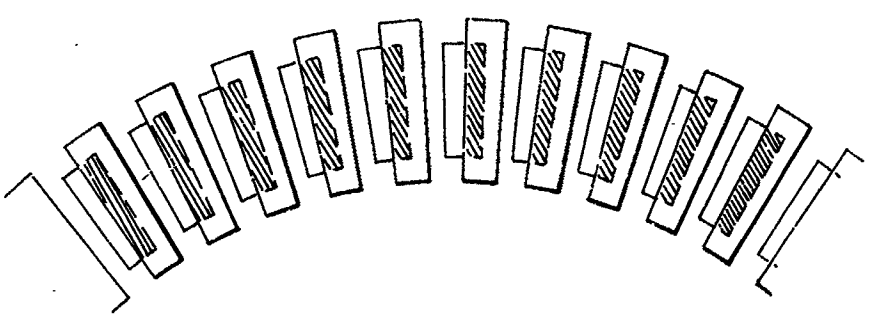

Figure 22. Vanes of Heliotropic System Viewed Along Axis of Symmetry

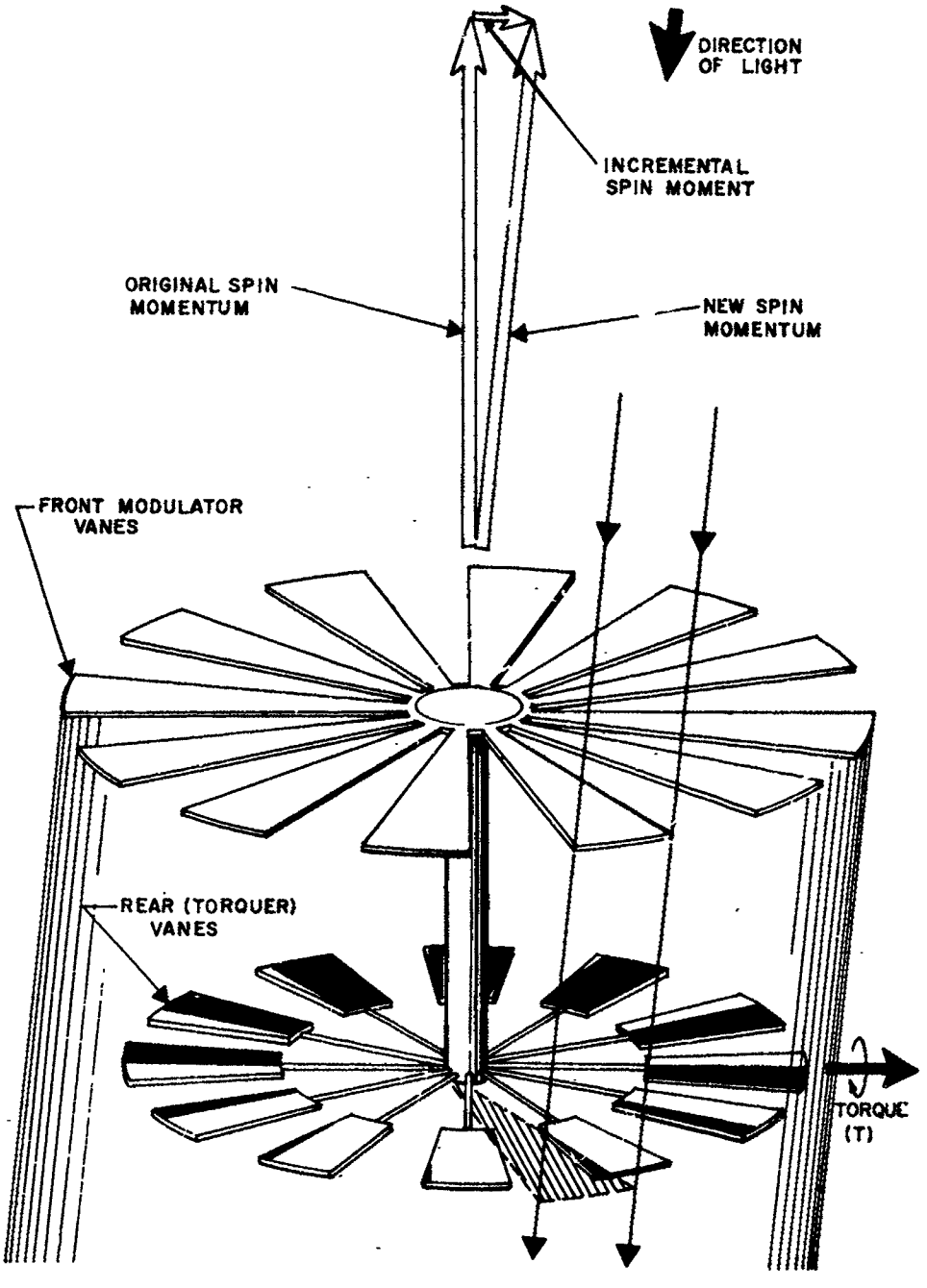

Figure 23. Schematic Heliotropic System

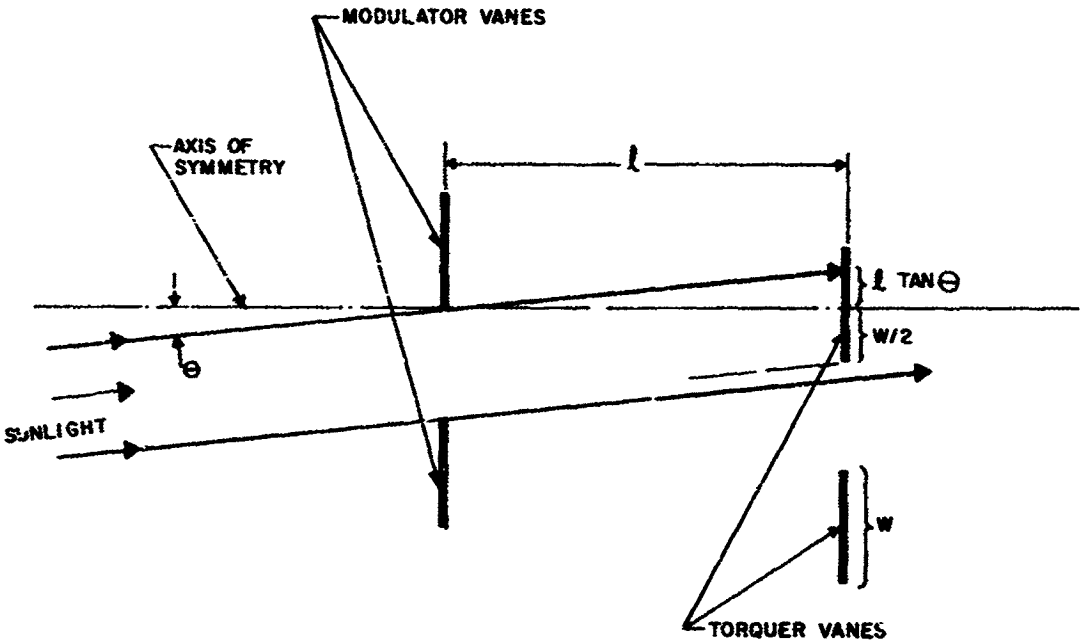

Figure 24. Geometry of Illumination of Heliotropic System

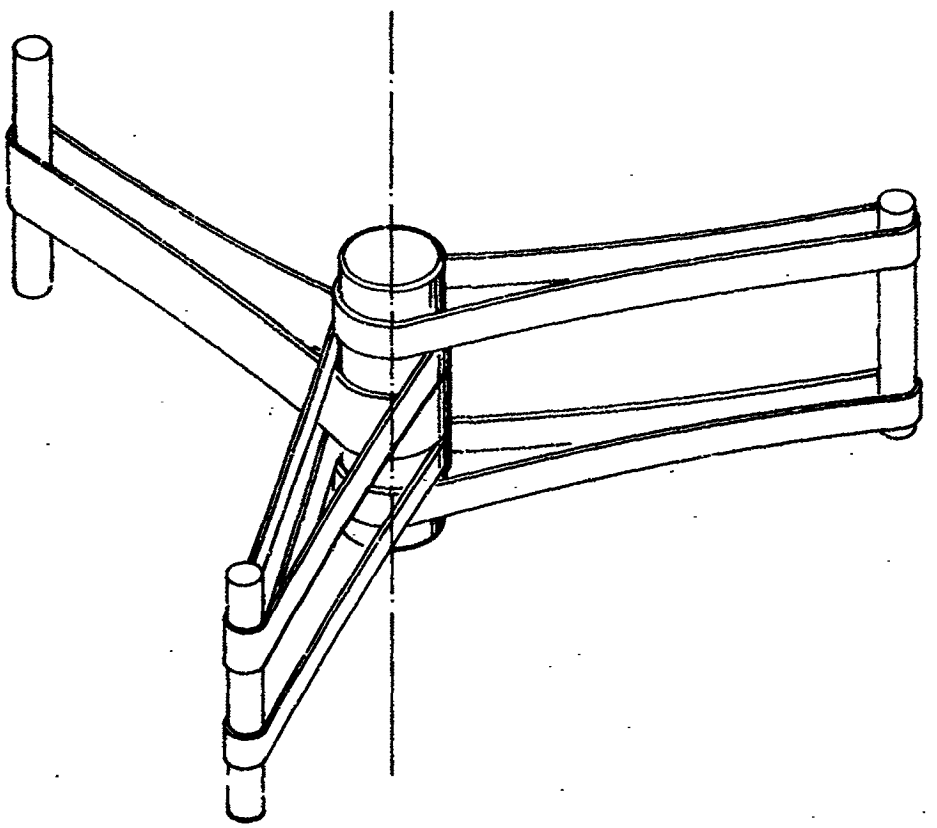

Figure 25. Overall View of Belt Radiator System

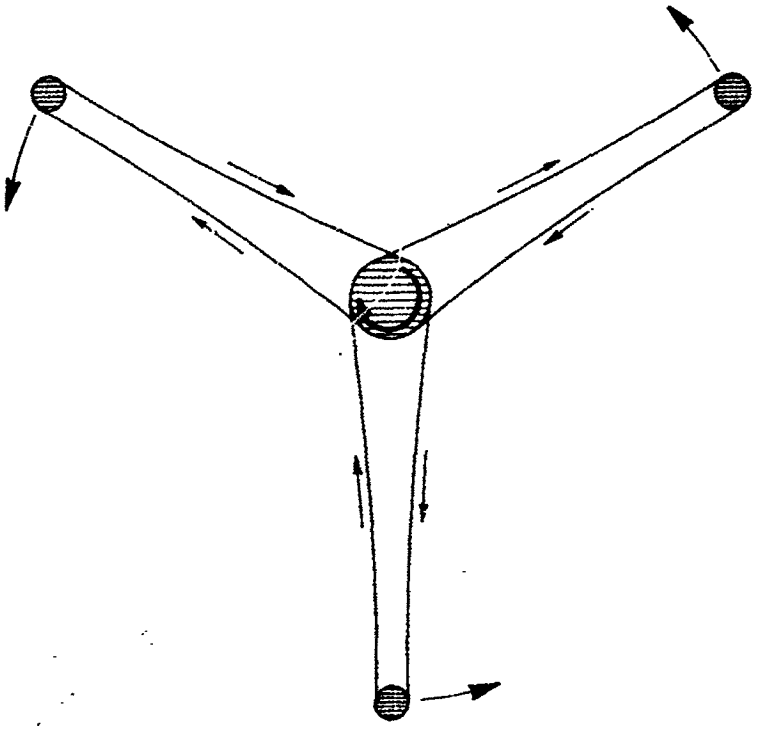

Figure 26. Motion of Belt System

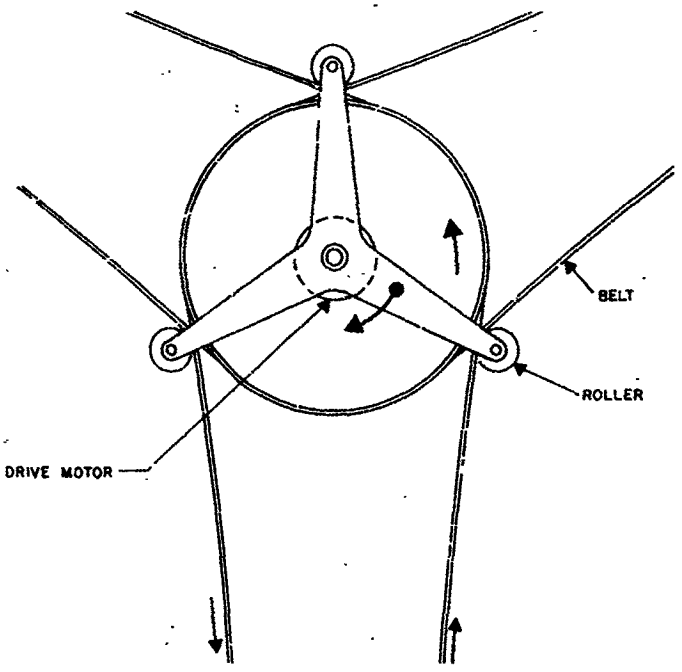

Figure 27. Belt Drive System Using Rollers

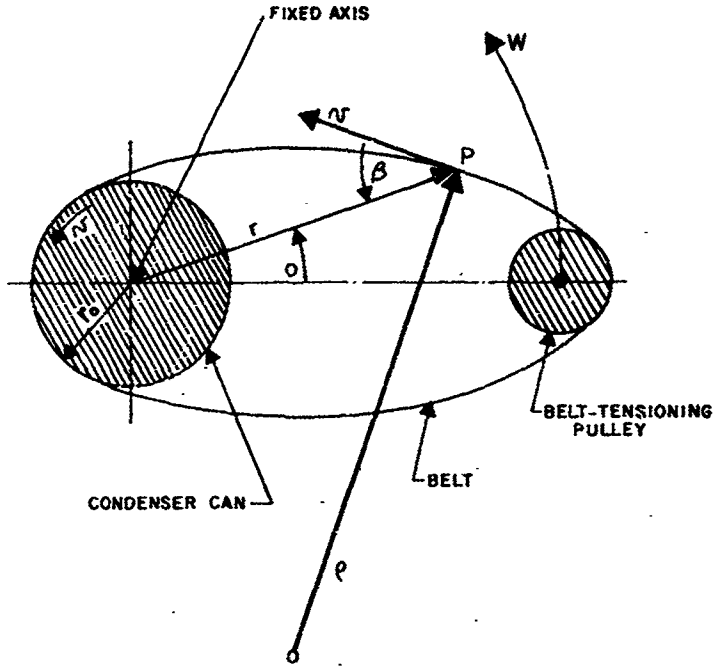

Figure 28. Geometry of Belt System

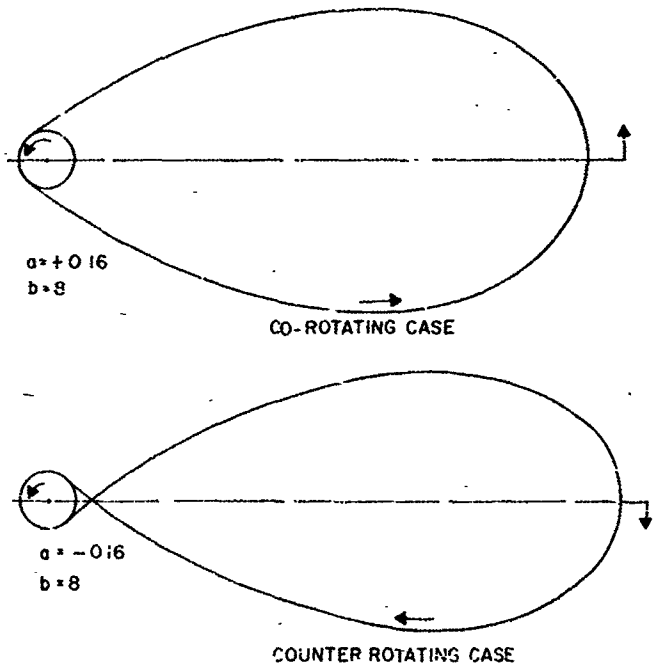

Figure 29. Two Examples of Belt Shape

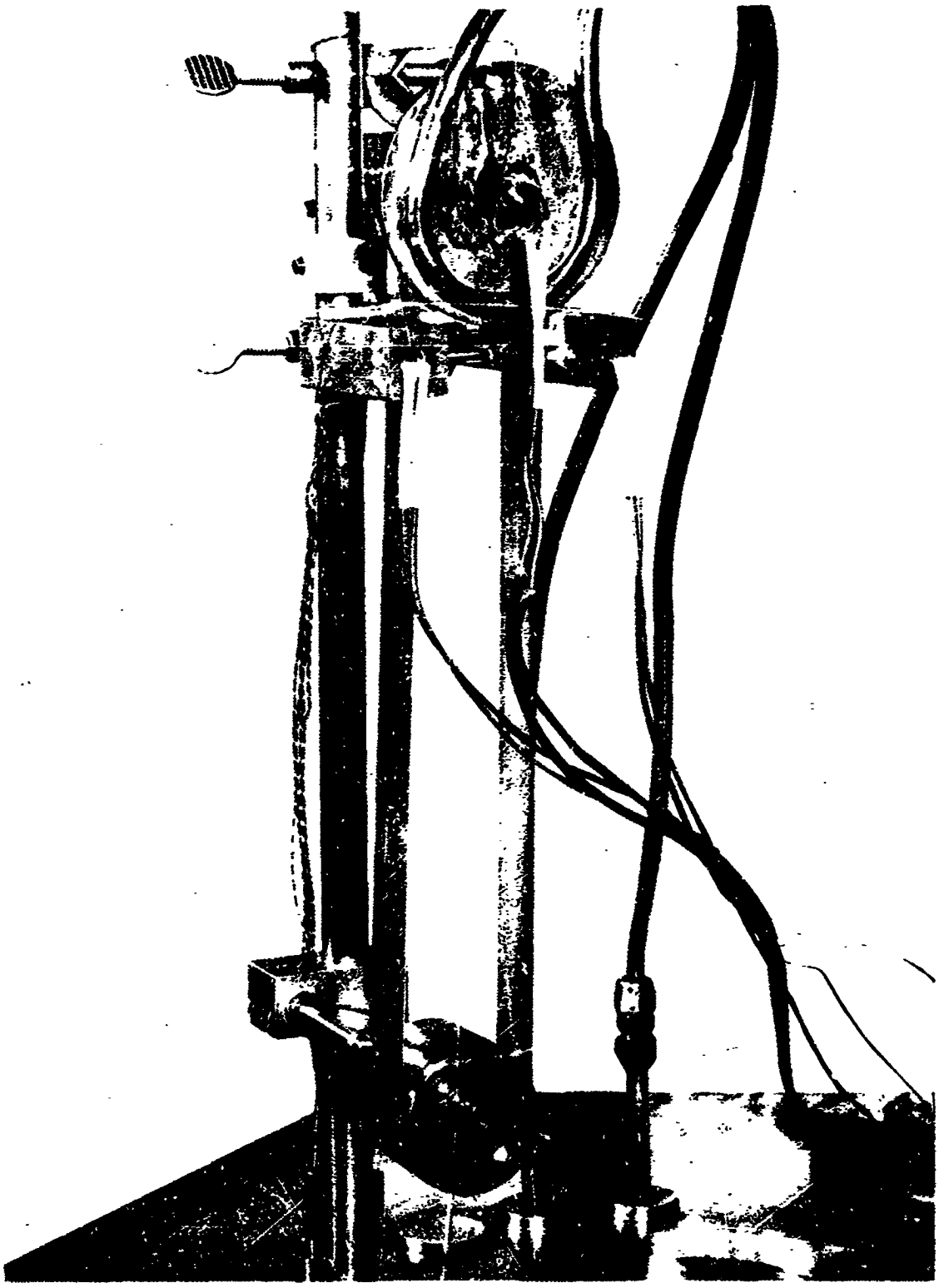

Figure 30. Belt Heat Transfer Experiment

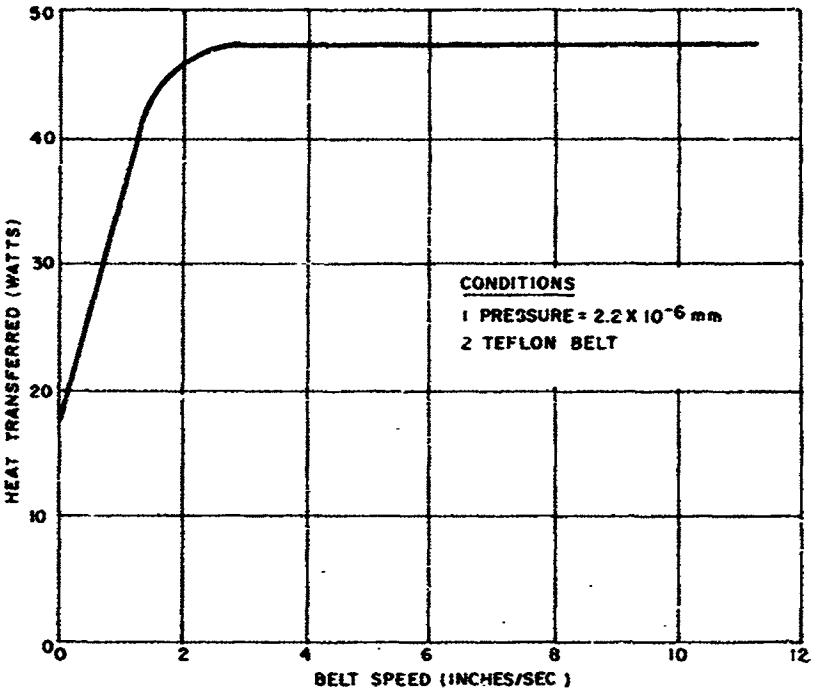

Figure 31. Heat Transferred from Pulley vs. Belt Speed

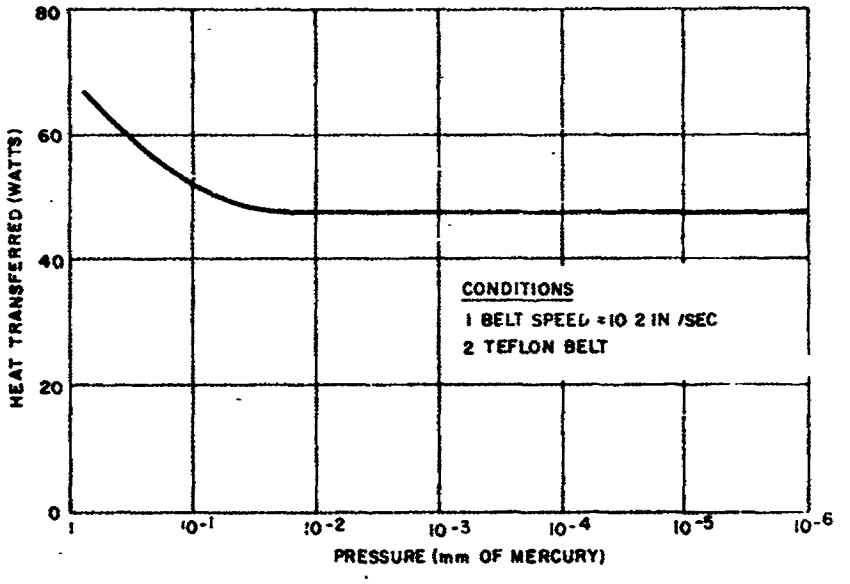

Figure 32. Heat Transferred from Pulley vs. Pressure

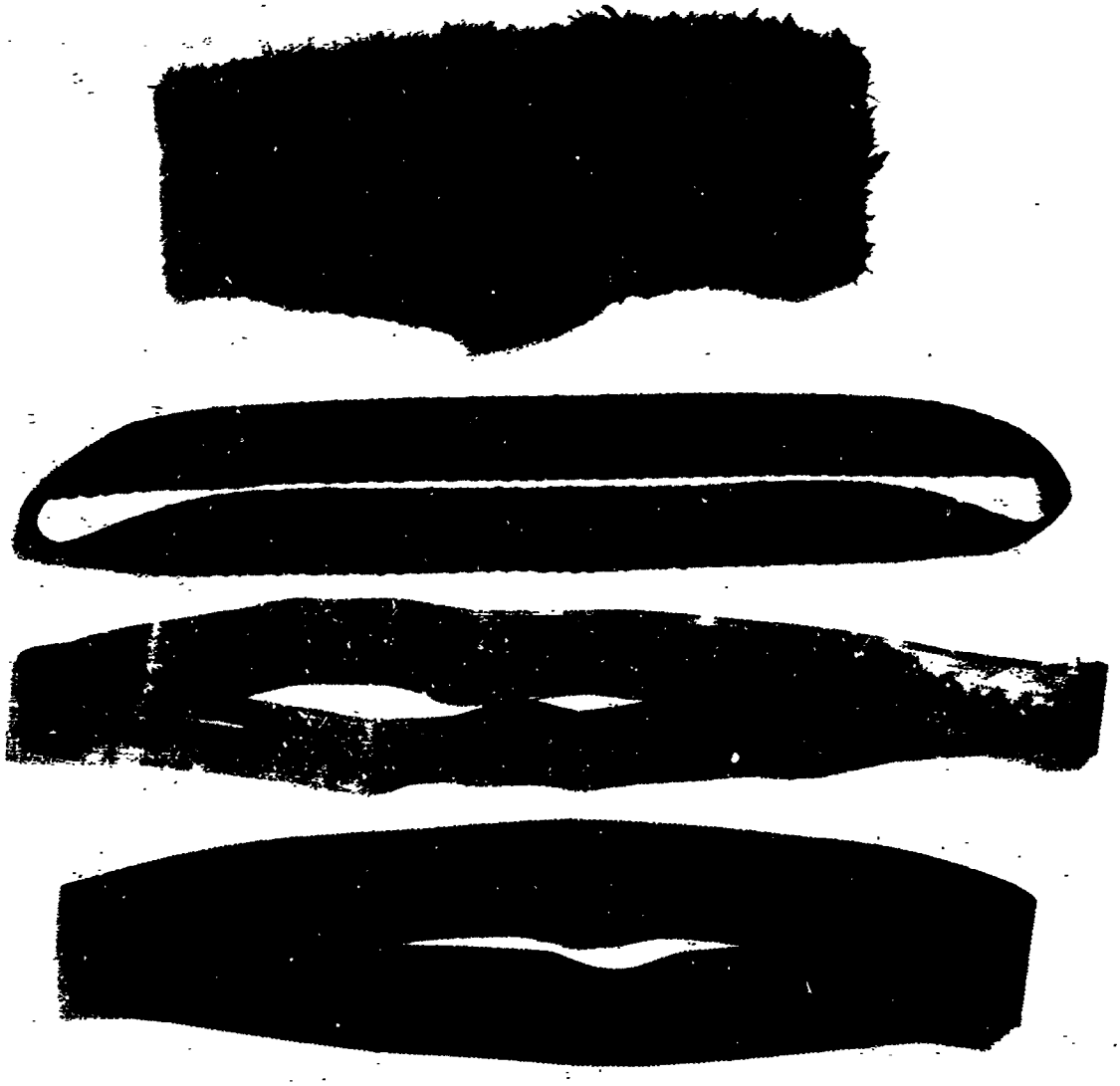

Figure 33. Belts Used in Heat Transfer Experiment

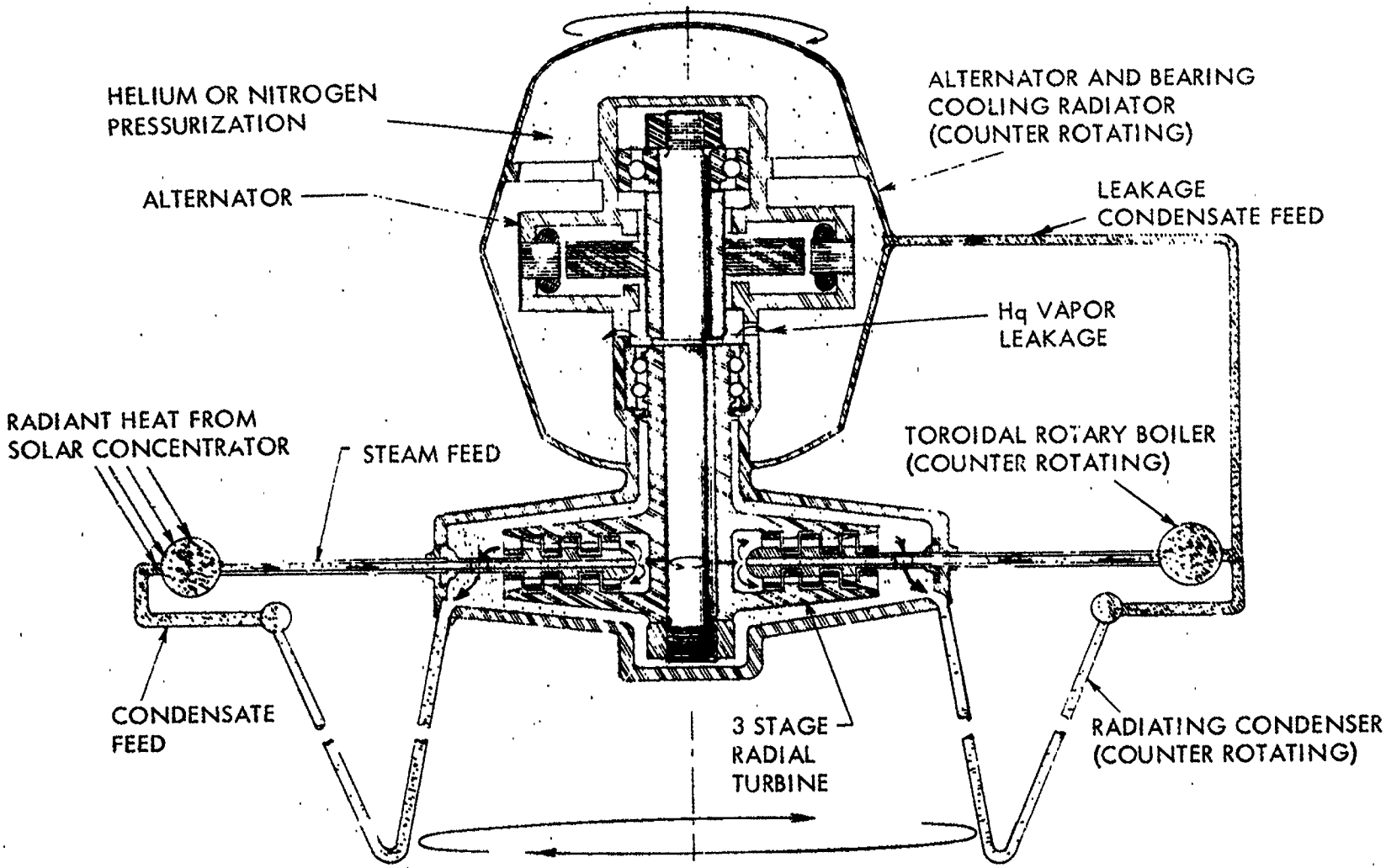

Figure 34. Schematic Presentation of Rotary Boiler -- Huettner Turbine

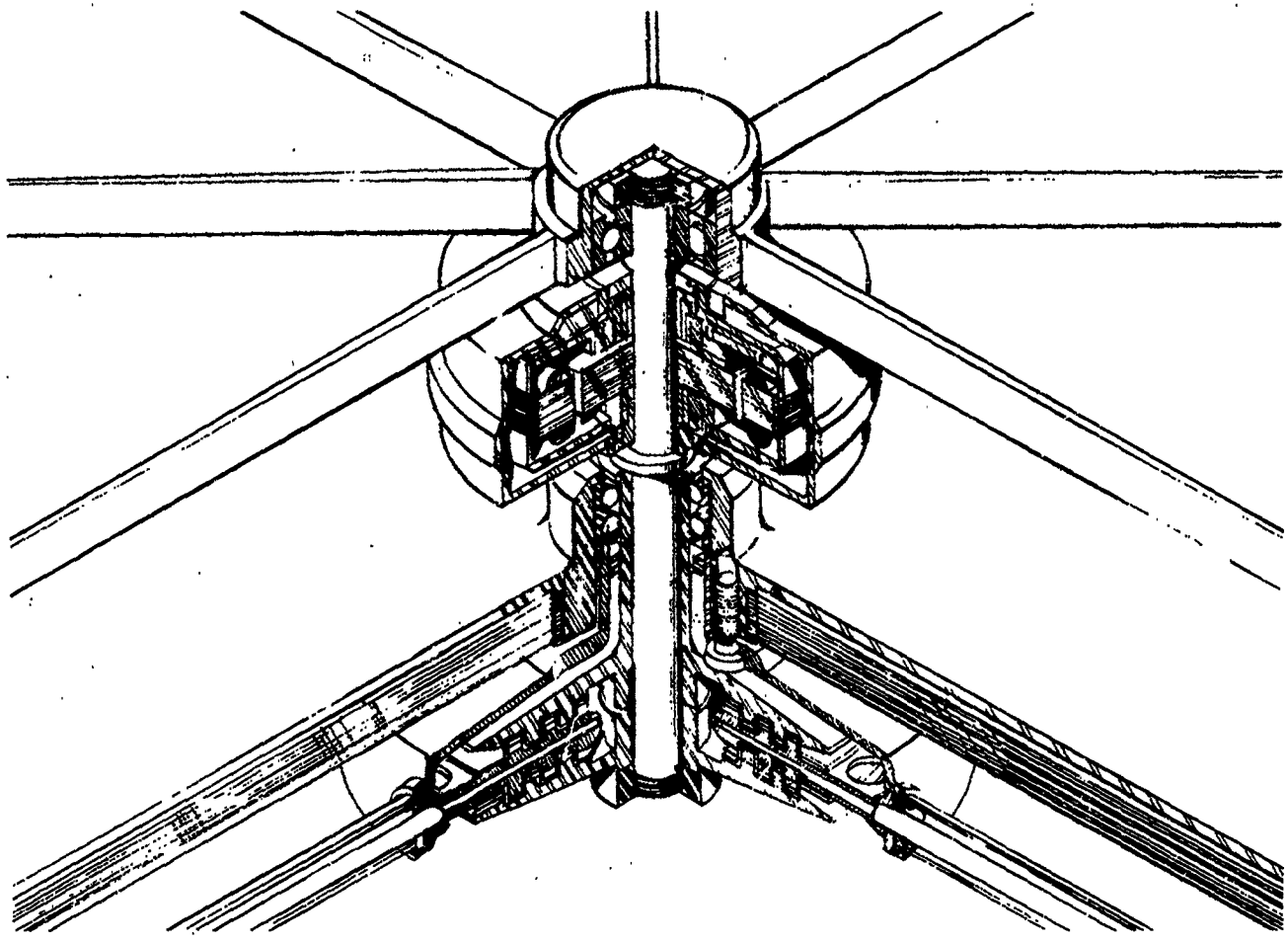

Figure 35. Turbine and Alternator

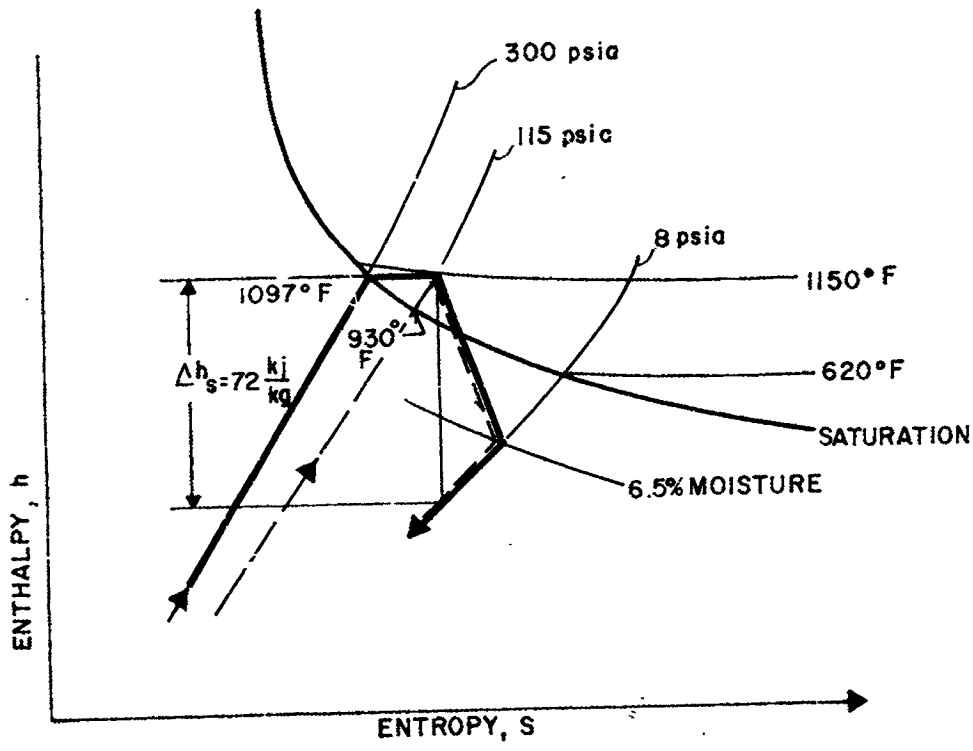

Figure 36. Enthalpy vs. Entropy Diagram for Huettner Turbine

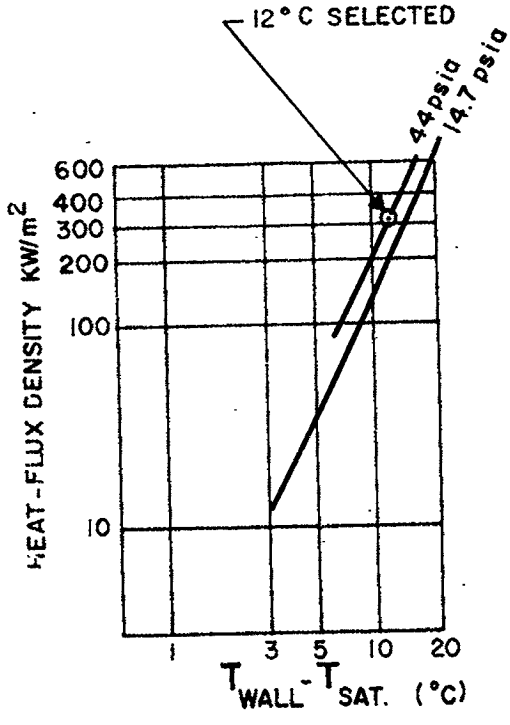

Figure 37. Heat Flux Density for Nucleate Boiling of Mercury

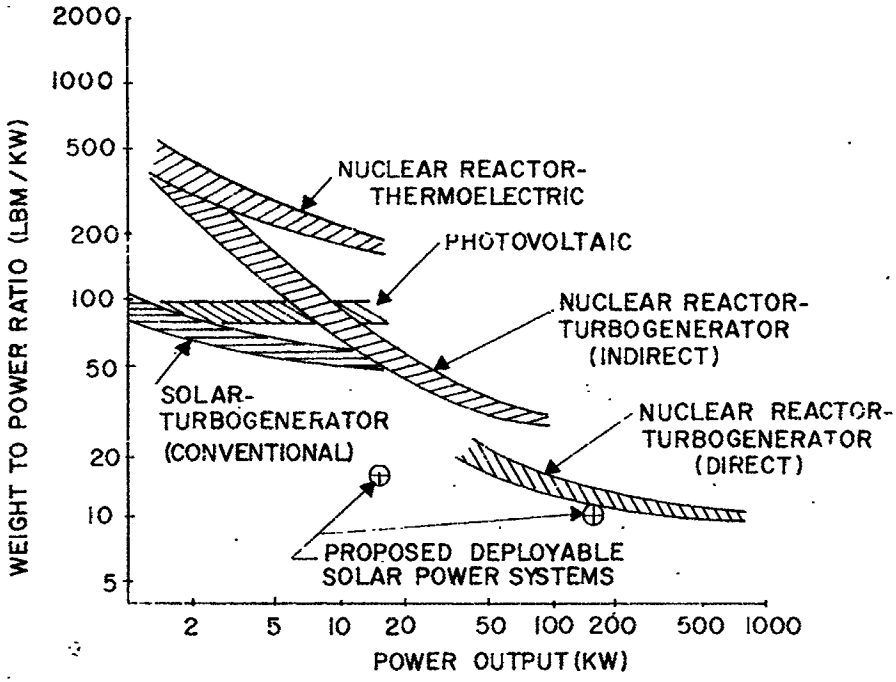

Figure 38. Weight-to-Power Ratio for Space Systems